

The Hubble Constant from Blue Type Ia Supernovae

CHRISTA GALL ¹, LUCA IZZO ^{2,1}, RADOSŁAW WOJTAK ¹, AND JENS HJORTH ¹

¹*DARK, Niels Bohr Institute, University of Copenhagen, Jagtvej 155A, DK-2200 Copenhagen N, Denmark*

²*INAF, Osservatorio Astronomico di Capodimonte, Salita Moiariello 16, I-80131 Napoli, Italy*

ABSTRACT

There is a persistent tension of about $5\sigma - 6\sigma$ between the value of the Hubble constant, as derived from the local distance ladder vs. the cosmic microwave background, signaling either unaccounted for systematics in the measurements or ‘new physics’, such as early dark energy. Determining the Hubble constant using Type Ia supernovae requires nontrivial and accurate corrections for dust extinction. To circumvent this obstacle, we here determine the Hubble constant from blue, and hence presumably unextinguished, supernovae. For two different sets of Type Ia supernova data and lightcurve fitting methods, we find that when using blue supernovae only, the derived Hubble constant is consistently lower by $\sim 3 \text{ km s}^{-1} \text{ Mpc}^{-1}$ (70 ± 2.1 and $70.3 \pm 3.0 \text{ km s}^{-1} \text{ Mpc}^{-1}$), and within 1σ of the cosmic microwave background measurement, compared to when using all supernovae. This is consistent with the hypothesis that systematic effects in dust corrections may affect standard supernova cosmology. However, the number of blue calibrating Type Ia supernovae is small (about six), and values of the Hubble constant for a range of different supernova colors are consistent at the 1.2σ level. Upcoming major transient surveys will discover numerous unextinguished SNe Ia, and thus be able to increase the precision of the Hubble constant measured from blue SNe Ia, heralding a promising path toward resolving the Hubble constant tension.

Keywords: Type Ia supernovae (1728) — Hubble constant (758)

1. INTRODUCTION

One of the most important scientific breakthroughs of the past few decades is the discovery of the acceleration in the expansion of the Universe (Schmidt et al. 1998; Riess et al. 1998; Perlmutter et al. 1999), i.e., the second derivative of the scale factor with respect to time. Despite this, nearly a century after the discovery of the expansion of the Universe (Lemaître 1927; Hubble 1929), there is disagreement about the true value of the present-day expansion rate, the Hubble constant (H_0 , i.e., the first derivative of the scale factor). Tension at a significance of about $5\sigma - 6\sigma$ arises between different independent measurements (Verde et al. 2019; Di Valentino et al. 2021; Calabrese et al. 2025). Most prominently, this is between that of ‘early Universe’ measurements of $H_0 = 67.36 \pm 0.54 \text{ km s}^{-1} \text{ Mpc}^{-1}$ (Planck Collaboration et al. 2020) based on the cosmic microwave background

(CMB) assuming a flat Λ cold dark matter cosmological model and the local $H_0 = 73.04 \pm 1.04 \text{ km s}^{-1} \text{ Mpc}^{-1}$ measurements (Riess et al. 2016, 2022a). The latter are based on the cosmic distance ladder involving observations of SNe Ia and Cepheids, which are calibrated with geometric distances to the Large Magellanic Cloud (Pietrzyński et al. 2019), Milky Way (Riess et al. 2021), or the megamaser galaxy NGC 4258 (Riess et al. 2022a; Freedman et al. 2019).

In this paper, we address the measurement of H_0 using SNe Ia as standardizable candles. SN Ia data sets cover a wide redshift range ($z < 2.26$) and are sufficiently large that statistical uncertainties are subdominant (Betoule et al. 2014; Brout et al. 2019; Riess et al. 2022a; Scolnic et al. 2022; Brout et al. 2022a; Möller et al. 2022; Vincenzi et al. 2024). It is therefore important to investigate if unaccounted-for systematic uncertainties could be the source of the discrepancy. SN Ia cosmology requires a range of corrections related to intrinsic luminosity and color variations at optical and near infrared wavelengths (Phillips et al. 1999; Mandel et al. 2009; Burns et al. 2014, 2018; Phillips et al. 2019; Dhawan

et al. 2023), extinction corrections (Riess et al. 1996; Jha et al. 2007; Mandel et al. 2017, 2011, 2022; Brout & Scolnic 2021; Dhawan et al. 2023), correlations with host-galaxy properties (Kelly et al. 2010; Sullivan et al. 2010), the progenitor systems and explosion mechanism of SNe Ia (Gall et al. 2018; Ashall et al. 2018) or astrophysical selection effects (Dainotti et al. 2021, 2022, 2025).

On the distance calibration, i.e., the anchoring of relative SN Ia distances, Cepheid variable stars (Leavitt & Pickering 1912, Leavitt Law), are often used to measure absolute distances to nearby SNe Ia (Freedman et al. 2001; Riess et al. 2016; Burns et al. 2018; Riess et al. 2022b). This method preferentially yields a high value of H_0 , largely consistent with what is found using other methods, including Surface Brightness Fluctuations (e.g., Tonry & Schneider 1988; Blakeslee et al. 2021; Garnavich et al. 2023), Tully–Fisher relation calibration (e.g., Tully & Fisher 1977; Schombert et al. 2020), or Fundamental Plane measurements (e.g., Scolnic et al. 2025), which, however, typically report larger systematic uncertainties. Measurements that are not in tension with the CMB value, e.g., H_0 of 69.85 ± 1.75 (stat) ± 1.54 (sys) $\text{km s}^{-1} \text{Mpc}^{-1}$ is reached using the Tip of the Red Giant Branch method (Madore & Freedman 1995; Freedman et al. 2019; Freedman 2021; Uddin et al. 2020; Freedman et al. 2025). Recently, with a new J-region asymptotic giant branch method, a value of $H_0 = 67.96 \pm 1.85$ (stat) ± 1.90 (sys) $\text{km s}^{-1} \text{Mpc}^{-1}$ has been found (Lee et al. 2024).

To determine the intrinsic brightness of an SN Ia, one needs to account for foreground dust extinction in its host-galaxy accurately. The degeneracy between the SN Ia intrinsic colors and extrinsic reddening due to line of sight host-galaxy extinction (Mandel et al. 2017; Brout et al. 2019; Brout & Scolnic 2021; Wojtak & Hjorth 2022) poses a significant challenge. Recent studies show that SNe Ia with very red observed colors lead to a larger rms scatter between the data and the best-fit model (e.g., Brout & Scolnic 2021; Popovic et al. 2023; Kelsey et al. 2021; Rose et al. 2022; Kelsey et al. 2023). Independent of the modeling and analysis approach, and whether or not additional correction steps (e.g., host-galaxy mass step) are included, the origin of this distribution is largely ascribed to variations in the total-to-selective-extinction parameter, R_V .

The parameter R_V essentially characterizes the dust properties along the line of sight to a supernova. In the Milky Way and neighboring galaxies (Cardelli et al. 1989; Schlafly et al. 2012, 2016; Fitzpatrick 1999; Calzetti et al. 1994; Zhang & Green 2025) the value of R_V ranges from around 2.5 to 6 for sight lines through

the diffuse to dense interstellar medium (ISM), with a mean of 3.1 and a fairly small scatter for the Milky Way. In cosmological analyses of SNe Ia, one typically finds values ranging from 1.5 to 3, with a broad gaussian distribution (e.g., mean $\sigma_{RV} > 1$, Popovic et al. 2023) and depending on the priors adopted for SN Ia intrinsic colors and reddening (Mandel et al. 2011; Burns et al. 2014; Mandel et al. 2017, 2022; Thorp & Mandel 2022; Thorp et al. 2021; Meldorf et al. 2023; Kelsey et al. 2023; Vincenzi et al. 2024; Popovic et al. 2024a; Grayling et al. 2024). Thorp et al. (2021) found values between 2.6 and 2.7, which are independent of the host-galaxy mass while other studies find a dependence on the mass of the host galaxies with larger mean R_V values of ~ 2.8 for lower mass galaxies and lower mean R_V values of ~ 1.5 for high mass galaxies (Brout & Scolnic 2021; Popovic et al. 2023). From the lightcurves of individual SNe Ia, extremely low $R_V = 1.5$ – 1.8 values have also been inferred for a handful of highly reddened SNe Ia, typically assuming a symmetric Gaussian prior for the SN Ia intrinsic color (Elias-Rosa et al. 2006, 2008; Wang et al. 2008; Amanullah et al. 2014).

A very small R_V could point to special dust properties in the vicinity of SNe Ia (Goobar 2008; Bulla et al. 2018), although they can be difficult to reconcile with known physical dust properties (Draine 2011). It remains puzzling that rarely larger R_V values are inferred, contrary to those commonly found in the sight lines of the Milky Way, in an SN Ia calibrator galaxy (Murakami et al. 2025), or in samples of star-forming galaxies (Calzetti et al. 1994; Keel et al. 2014; De Marchi et al. 2020, 2021). Alternatively, the effect may be due to an inadequate treatment of SN Ia colors (Guy et al. 2010; Burns et al. 2011). More fundamental issues inherent to differences in the intrinsic and extrinsic color distribution of different populations of SN Ia in the different SN Ia samples may also exist (e.g., Wojtak & Hjorth 2025a; Rubin et al. 2026). As demonstrated by Mandel et al. (2017, 2022), disentangling intrinsic color variations within the SN population from dust reddening to a cosmologically relevant precision remains challenging. An entirely different approach to describe the intrinsic and extrinsic reddening effects may be needed (Wojtak et al. 2023; Wojtak & Hjorth 2024; Popovic et al. 2024b).

In principle, SN cosmology would not depend on the details of dust corrections in the ideal situation where calibration and HF samples would be drawn from strictly identical SN and host-galaxy populations in an unbiased way. Riess et al. (2022a) carefully selected samples with similar properties (blue spiral galaxies). However, for precision cosmology, one cannot rule out second-order effects (Wojtak & Hjorth 2024).

A promising avenue to eliminate the effects of reddening is to study SNe Ia in the near-infrared (NIR), where dust extinction is suppressed relative to the blue–optical range. From modeling data in optical + NIR, [Dhawan et al. \(2023\)](#) found $H_0 = 74.82 \pm 0.97$ (stat) ± 0.84 (sys) $\text{km s}^{-1} \text{Mpc}^{-1}$ when using the calibration with Cepheid distances to 37 host galaxies of 41 SNe Ia, and 70.92 ± 1.14 (stat) ± 1.49 (sys) $\text{km s}^{-1} \text{Mpc}^{-1}$ when using the calibration with tip of the red giant branch distances to 15 host galaxies of 18 SNe Ia. [Galbany et al. \(2023\)](#) found $H_0 = 72.3 \pm 1.4$ (stat) ± 1.4 (sys) $\text{km s}^{-1} \text{Mpc}^{-1}$ in the J band and $H_0 = 72.3 \pm 1.3$ (stat) ± 1.4 (sys) $\text{km s}^{-1} \text{Mpc}^{-1}$ in the H band.

Considering the challenges in establishing a universally applicable and physical dust model for SN Ia cosmology, in this paper we take a complementary approach. We attempt to circumvent dust corrections entirely by only studying the bluest SNe Ia, which is presumably the least reddened subpopulation of SNe Ia ([Mandel et al. 2017](#); [Wojtak et al. 2023](#); [Wojtak & Hjorth 2024](#); [Popovic et al. 2023, 2024a](#)). We show that there is a dependence of H_0 on SN Ia color, with the bluest SNe Ia leading to values that are not strongly discrepant with the low CMB H_0 value (and at the same time not inconsistent with the SH0ES value). Section 2 briefly describes the publicly available data sets and methods used in this work. In Section 3 we demonstrate that lower values of H_0 are obtained for blue SNe Ia in two different samples. We discuss the results and impact thereof on the H_0 -tension in Section 4 and conclude that a promising way of dealing with uncertain dust corrections in addressing the H_0 -tension may be to focus on unextinguished SNe Ia only.

2. DATA AND ANALYSIS

We use SN Ia data that are acquired by different surveys, and for which SN Ia lightcurve parameters are obtained from two distinct lightcurve fitters as described below. SN Ia peak magnitudes are calibrated using common empirical relations between the SN Ia peak luminosity and lightcurve parameters describing either the decline rate or shape of it ([Phillips 1993](#)) as well as the luminosity-color relation ([Tripp 1998](#)). To obtain H_0 , the intrinsic peak magnitudes and other model parameters (see Sect. 2.2), we use Bayesian inference modeling to fit model parameters using Markov Chain Monte Carlo (MCMC) sampling.

2.1. *Pantheon+*, *SH0ES* and SALT

We take SN Ia lightcurve parameters from the recent comprehensive Pantheon+ SN Ia compilation together with the full cosmological model setup as described in

[Brout et al. \(2022a\)](#). In alignment with this, we use the Cepheid distances to 42 calibrating SNe Ia hosted in 37 individual galaxies as observed through the Supernovae and H0 for the Equation of State of dark energy (SH0ES) program ([Riess et al. 2016, 2022a](#)).

Pantheon+ comprises SN Ia data taken from several SN Ia surveys, such as the Harvard Smithsonian Center for Astrophysics (CfA1–4 [Riess et al. 1999](#); [Jha et al. 2006](#); [Hicken et al. 2009b, 2012, 2009a](#)) and the Carnegie Supernova Project (CSP-I [Contreras et al. 2010](#); [Folatelli et al. 2010](#); [Stritzinger et al. 2011](#)), some are also compiled in the Open Supernova Catalog ([Guillochon et al. 2017](#)). Pantheon+ is the successor of the SuperCal supernova compilation ([Scolnic et al. 2015](#)), used by [Riess et al. \(2016\)](#) to obtain the Hubble constant measurement, which indicated for the first time a discrepancy (3.4σ) with the value derived from the Planck observations of the CMB.

The SN Ia lightcurve parameters have been obtained through a retrained Spectral Adaptive Lightcurve Template (SALT2) model ([Guy et al. 2007, 2010](#); [Scolnic & Kessler 2016](#); [Taylor et al. 2021](#); [Brout et al. 2022b](#)). The cosmological model is based on and adjusted to using SALT2 SN Ia lightcurve parameters together with the [Tripp \(1998\)](#) calibration. The distance modulus is computed as

$$\mu = m_B - M_B + \alpha x_1 - \beta c - \delta_{\text{bias}} + \delta_{\text{host}}, \quad (1)$$

with M_B the absolute B -band peak magnitude, and x_1 and c the SALT2 specific lightcurve parameters characterizing the shape and color of the SN lightcurves, and α and β as linear correction coefficients, which are fitted parameters in the cosmological model.

Using SALT2 ([Guy et al. 2005, 2007](#)), the color is defined as the rest-frame $B - V$ color with respect to the average at maximum B -band brightness as $c = (B - V)_{\text{max}} - \langle B - V \rangle$. Then, c represents the phase-independent total color difference of an SN (i.e., extrinsic extinction and intrinsic SN color variation) with respect to the mean color, assumed $\langle B - V \rangle = 0$, of the SALT2 training sample. The latter is an inhomogeneous compilation of low and high redshift SNe Ia from different observations ([Guy et al. 2005, 2007](#), and references therein).

Besides the standard lightcurve shape and color correction parameters, x_1 and α , additional corrections are included. The δ_{bias} accounts for observational selection biases determined from simulations and corrections determined from modeling of dust and supernova intrinsic color ([Popovic et al. 2021, 2023](#)). The term, δ_{host} , accounts for potential residual correlations between the host-galaxy mass and the standardized brightness of

SN Ia (Eq. 4, Brout et al. 2022a). The distance modulus uncertainty, for this model, accounts for uncertainties from observational selection effects, measurement uncertainties of lightcurve parameters, peculiar velocities, gravitational lensing, redshift measurements, and intrinsic variations of SNe Ia. A detailed description of the uncertainties and associated covariances is presented in Brout et al. (2022a, and references therein).

For the purpose of this work, we adopt the already corrected SN Ia peak magnitudes, $m_{B,\text{corr}}$, as derived from the model of supernova standardization (Eq. 1, Brout et al. (2022a)) together with the covariance matrix for all SN Ia corrected peak magnitudes and distance moduli, made publicly available¹. The entire Pantheon+ data set consists of 1701 entries in total, 1546 SNe Ia, including the calibrator SNe Ia within a redshift range $0.00122 < z < 2.26137$. To be consistent with H_0 measurements in the literature, we select the same Hubble flow (HF) SNe Ia that obey the data selection criteria (SNe Ia with late-type hosts similar to those of the Cepheid calibrators, $0.023 < z < 0.15$; $|c| < 0.15$; $|x_1| < 2$; $\sigma_{t_{\text{PEAK}}} < 5$ days; $\sigma_{m_B} < 0.2$ mag) as used by the SH0ES team and outlined in Riess et al. (2022a).

We refer to this as the HF sample, which has a total of 270 entries for 234 individual SNe Ia. For this work, we develop a custom-made Python code that makes use of publicly available Python codes¹ to select SNe Ia and build respective covariance matrices for each color bin.

The corrected SN Ia peak magnitude is defined as

$$m_{B,\text{corr}} = M_B + \mu, \quad (2)$$

where $\mu = \mu(z)$ is a cosmology-dependent distance modulus for SNe Ia in the Hubble flow and $\mu = \mu_{\text{ceph}}$ is a distance modulus measured from Cepheid observations for SNe Ia in the calibration galaxies.

The combined likelihood as defined by Brout et al. (2022a) is

$$-2 \ln L = \Delta \vec{D}^T (C_{\text{stat+sys}}^{\text{cos}} + C_{\text{stat+sys}}^{\text{cal}})^{-1} \Delta \vec{D}, \quad (3)$$

with $D_i = \mu_i - \mu_{\text{ceph},i}$ for SNe, i , in the calibration galaxies, $D_i = \mu_i - \mu(z_i, H_0)$ for SNe, i , in the Hubble flow, where

$$\mu(z_i, H_0) = \mu_{\text{Planck}}(z_i) + 5 \log_{10} \frac{H_0}{H_{0,\text{Planck}}}, \quad (4)$$

leaving the absolute B -band magnitude, M_B , and H_0 as the only two free parameters to be fit. The statistical

and systematic covariance for the cosmological sample is denoted $C_{\text{stat+sys}}^{\text{cos}}$ and $C_{\text{stat+sys}}^{\text{cal}}$ for the Cepheid calibrated SN Ia host galaxies. The subscript Planck refers to quantities taken from the Planck cosmological model (Planck Collaboration et al. 2020) as implemented in `python astropy`. To find the best-fit model parameters, we use the MCMC sampling technique as implemented in the Python package `emcee` (Foreman-Mackey et al. 2013).

2.2. CSP-I and CSP-II, SH0ES and SNOOPy

We adopt the B -band SN Ia lightcurve parameter of SNe Ia lightcurve data compiled by CSP-I & II (Kriszunas et al. 2017; Phillips et al. 2019; Uddin et al. 2020) and the cosmological model from Uddin et al. (2024). All SNe Ia lightcurve data have consistently been fit with the SNOOPy lightcurve fitter (Burns et al. 2011, 2014) using the integrated ‘max-model’ to obtain the peak B - and V -band magnitudes (m_B , m_V) and the lightcurve color-stretch parameter s_{BV} as described also in Uddin et al. (2024). The SN Ia colors are calculated as pseudocolors ($B_{\text{max}} - V_{\text{max}}$). We use the SN Ia data, the calculated covariance matrix, and host-galaxy information as made available on GitHub². For consistency with the SN Ia selection concept of Pantheon+ (Sect. 2.1), we select HF SNe Ia within a color range of the calibrator sample (i.e., $|(B - V)| < 0.22$ mag), a color stretch parameter $s_{BV} > 0.6$ and with a redshift > 0.0233 , which results in a final HF data set of CSP-I and CSP-II 177 SNe Ia out of a total of 322 SNe Ia used in Uddin et al. (2024). The $(B - V)$ and s_{BV} parameter value ranges for the HF sample are chosen to be close to those encompassed by the SNe Ia in the calibrator sample. The lower bound on s_{BV} excludes subluminous, fast-declining SN Ia subtypes (e.g., Gall et al. 2018). We find that out of the 177 HF SNe Ia used here, only 29 SN Ia are also in the Pantheon+ compilation (Sect. 2.1) of which 27 are from the CSP-I sample. Due to this, the HF SN Ia sample here can be considered an ‘almost independent data set’. We use the Cepheid distances from the SH0ES program (Riess et al. 2022a) to 25 CSP SNe Ia of Uddin et al. (2024).

The apparent rest-frame B -band peak magnitudes are modeled as

$$m_B = P^0 + P^1(s_{BV} - 1) + P^2(s_{BV} - 1)^2 + R(B_{\text{max}} - V_{\text{max}}) + \zeta(M - \bar{M}) + \mu, \quad (5)$$

where P^0 , P^1 and P^2 are parameters of the polynomial $P^N(s_{BV}) - 1$ of the luminosity-decline rate rela-

¹ <https://github.com/PantheonPlusSH0ES/DataRelease/tree/main>

² <https://github.com/syeduddin/h0csp>

tion up to second order ($N = 2$). Additionally, R is the color correction parameter, which is the slope of the luminosity-color relation and ζ is the global slope parameter of the luminosity-host-galaxy stellar mass, $M = \log_{10}(M_*/M_\odot)$, correction with \bar{M} , denoting the median value of the host-galaxy stellar mass of a sample of SNe Ia. Then, $\mu = \mu_{\text{ceph}}$ is the distance modulus of SNe Ia in the Cepheid calibration sample. In order to obtain the Hubble constant, H_0 , μ in Eq. 5 is replaced by a distance modulus as a function of redshift and H_0 with the model distance modulus for SNe Ia is as defined in Burns et al. (2018),

$$\mu(z_{\text{hel}}, z_{\text{CMB}}, H_0) = 5 \log_{10} \left[\left(\frac{1 + z_{\text{hel}}}{1 + z_{\text{CMB}}} \right) \frac{cz_{\text{CMB}}}{H_0} \left(1 + \frac{1 - q_0}{2} z_{\text{CMB}} \right) \right] + 25, \quad (6)$$

with the deceleration parameter, $q_0 = -0.53$ and z_{CMB} and z_{hel} the redshifts relative to the CMB and the heliocentric frame of reference, respectively.

As in Sect. 2.1, we use $\mu = \mu_{\text{ceph}}$ for SNe Ia in the Cepheid calibration sample and $\mu = \mu(z_{\text{hel}}, z_{\text{CMB}}, H_0)$ to obtain H_0 . The combined log-likelihood $\ln \mathcal{L} = \ln \mathcal{L}_{\text{cal}} + \ln \mathcal{L}_{\text{cos}}$ is then

$$\Gamma_X = \frac{(m_B - m_{B,\text{model}})^2}{\sigma_{\text{tot}}^2},$$

$$\sigma_{\text{tot}}^2 = \sigma_X^2 + \sigma_{\text{int}}^2 + \sigma_Y^2,$$

$$\ln \mathcal{L}_X = -\frac{1}{2} \sum_i^{N_X} \Gamma_{X,i} - \frac{1}{2} \sum_i^{N_X} \ln 2\pi\sigma_{\text{tot},i}^2. \quad (7)$$

The subscript, X , refers to either the calibration or cosmology (i.e., HF SN Ia) sample. Then, m_B is the observed B -band magnitude for each supernova and $m_{B,\text{model}}$ the intrinsic model magnitude as given in Eq. 5. The error term σ_X^2 represents the total uncertainties of all observed quantities and is as defined in Eq. 5 in Uddin et al. (2024),

$$\begin{aligned} \sigma_X^2 &= \sigma_{m_B}^2 + (P^1 + 2P^2(s_{BV} - 1))^2 \sigma_{s_{BV}}^2 \\ &+ R^2 \sigma_{(B-V)}^2 - 2(P^1 + 2P^2(s_{BV} - 1)) \text{cov}(m_B, s_{BV}) \\ &+ 2R(P^1 + 2P^2(s_{BV} - 1)) \text{cov}(s_{BV}, (B - V)) \\ &- 2R \text{cov}(m_B, (B - V)) + \zeta^2 \sigma_M^2. \end{aligned} \quad (8)$$

The error term σ_{int}^2 is calculated for the SNe Ia in the HF sample only and is the intrinsic scatter (included as a fit parameter). The error term $\sigma_Y^2 \equiv \sigma_{\mu,\text{ceph}}^2$ is used for the calibration sample and $\sigma_Y^2 \equiv \sigma_{\text{pec}}^2$ is the uncertainty due to peculiar velocities, $\sigma_{\text{pec}} = 2.17(v_{\text{pec}}/cz_{\text{cmb}})$, with v_{pec} representing the average peculiar velocity dispersion in the SN Ia HF sample, as a free parameter.

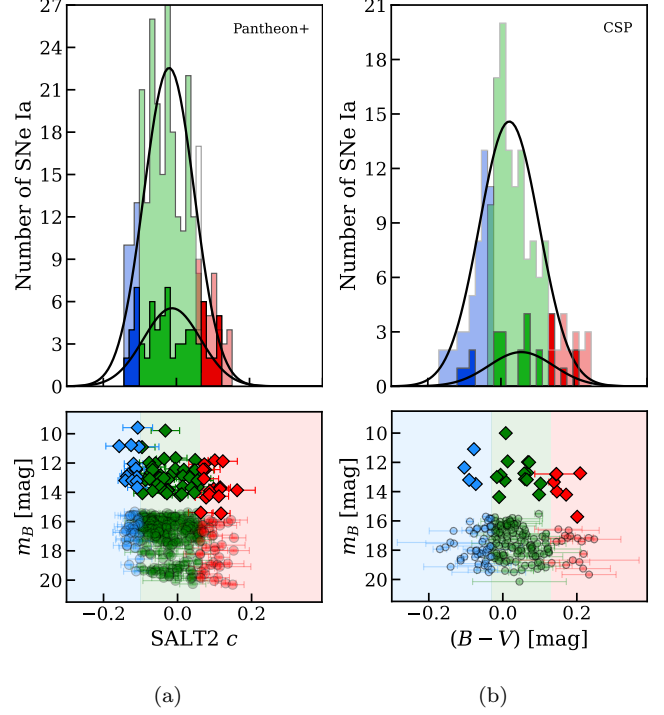


Figure 1. Number of SNe Ia (top row) and their measured peak magnitudes (bottom row) as a function of color. Shown are SNe Ia from Pantheon+ (a) and SNe Ia from CSP (b). Blue, green, and red colors mark the color range of the three color bins. The black solid lines are fit normalized probability density functions for each the HF and the calibrating SN Ia sample. Solid-filled diamonds / histograms represent the calibration SNe Ia while shaded filled circles / histograms represent SNe Ia in the HF sample.

In total, there are eight model parameters to be fit ($P^0, P^1, P^2, R, \zeta, \sigma_{\text{int}}, v_{\text{pec}}$ and H_0). We assume Gaussian priors and we use the MCMC sampling technique as implemented in the Python package `emcee` (Foreman-Mackey et al. 2013).

3. THE HUBBLE CONSTANT FROM BLUE SUPERNOVAE

We define three discrete color bins into which we divide the calibration and HF SN Ia data sets. For both Pantheon+ and CSP, the red and blue color cuts are chosen to contain only the bluest and reddest SNe Ia in the tail of the color distribution of the entire calibrating SN Ia sample. For Pantheon+ we consider all SNe Ia with a measurement of $c < -0.1$ mag as blue, nearly unextinguished SNe Ia. This is similar to the modeling-based estimate of the mean intrinsic color of

Table 1. Sample Definition Criteria

Model ^a	SN Ia Color Range ^b			# SNe Ia ^c				f_{SN} ^d			# SNe Ia ^e	
	Blue	Green	Red	Blue	Green	Red	All	Blue	Green	Red	Set 1	Set 2
Pantheon+	$C < -0.1$	$-0.1 < C < 0.06$	$C > 0.06$	6/28	25/176	11/35	17.9	21.4	14.5	32.4	239	29
CSP	$C < -0.03$	$-0.03 < C < 0.13$	$C > 0.13$	4/49	14/113	7/15	14.1	8.2	12.4	46.7	29	177

^aAll SNe sets are selected in the redshift range $0.0233 < z < 0.15$

^bFor Pantheon+, C is the SALT2 lightcurve fitting parameter c while for CSP, C denotes the $(B - V)$ [mag] color.

^cNumber of SNe Ia in the calibration / cosmology sample.

^d $f_{SN} = (N_{calib}/N_{cosmo}) \times 100$, with N_{calib} the number of calibrating SNe Ia and N_{cosmo} , the number of SNe Ia in the cosmological sample.

^eTotal number of SNe Ia that are in Pantheon+ (Set 1) and CSP (Set 2).

References— Riess et al. (2016) Riess et al. (2022a) Brout et al. (2022a) Uddin et al. (2024)

the Pantheon+ sample ($\bar{c} = -0.077 \pm 0.006$; Popovic et al. 2023).

However, Pantheon+ contains several duplicates, i.e. multiple entries of the same SN Ia with lightcurve parameters derived from lightcurve data obtained by different telescopes and/or instruments. While any possible systematics arising from this are dealt with and accounted for in the statistical and systematic covariance matrix $C_{stat+sys}^{cos}$ and $C_{stat+sys}^{cal}$ (Brout et al. 2022b; Scolnic et al. 2022), some such SNe Ia have color measurements with c values over a wide range. For example, in Pantheon+ we find five SNe Ia in each the calibration and the HF SN Ia sample with c measurements in both the blue and green color bin, and three SNe Ia in the calibration and HF SN Ia sample with c measurements in both the green and the red color bin. To avoid having the same SN Ia in two color bins, we calculate the weighted mean color of SNe Ia with multiple color measurements, and we use this weighted mean to decide in which color bin an SN Ia can be placed. We then use the measurement of the respective SN Ia in this color bin. The total number of SNe Ia in each color bin is summarized in Table 1.

The CSP and SALT color definitions are not identical (see Sect. 2). From the probability density function fits to the data compilations, as shown in Figure 1 the distribution of the calibration sample peaks at $\bar{c}_{cal} = -0.012 \pm 0.078$ mag for Pantheon+ while for CSP $\overline{B - V}_{cal} = 0.057 \pm 0.14$ mag, which corresponds to a difference in mean peak color between the two distributions of about 0.07 mag. To be in agreement with Pantheon+, the blue color cut of Pantheon+ would translate into a blue color cut for CSP to $B - V = -0.03$ mag, and

on the red side, $B - V = 0.13$ mag, which we adopt. Alternatively, the difference in the mean peak color between the two distributions of the HF samples is about 0.04 mag. This translates into a CSP blue and red color bound of $B - V = -0.06$ and $B - V = 0.10$, respectively. Results are shown in Appendix A.

The HF sample is split into color bins with the same color cuts as the calibration sample. However, the color distributions of SNe Ia in both the calibration and the HF samples are not identical. Thus, the ratio between the number of SNe Ia in different color bins is different between the calibration and the HF samples. A summary is presented in Table 1 and visualized in Figure 1.

Figure 2 shows H_0 as a function of the color bin for our two samples. For H_0 there is a clear ‘blue-to-red’ dependency on SN color in both cases. The upper panel shows that SNe Ia (Pantheon+) in the blue bin leads to a low $H_0 = 70.0 \pm 2.1$ km s⁻¹ Mpc⁻¹ while SNe Ia in the green bin yield the highest H_0 values of 74.5 ± 1.2 km s⁻¹ Mpc⁻¹. SNe Ia in the red bin also result in an H_0 value of 72.5 ± 2.7 km s⁻¹ Mpc⁻¹. H_0 obtained with SNe Ia in the green and red color bins are consistent with H_0 obtained for the entire sample, and both are consistent with standard SN Ia H_0 values in the literature (Riess et al. 2016, 2022a). All H_0 values can be considered consistent at a 1.2 σ level.

Nevertheless, the H_0 blue-to-red dependency on SN Ia color is intriguing, considering that the corrected peak magnitudes and covariance matrix (Brout et al. 2022a) already include various corrections (see Sect. 2.1). These are an SN Ia color and dust-based color law which depends on host-galaxy properties (Brout & Scolnic 2021; Popovic et al. 2021, 2023). Interestingly, using a differ-

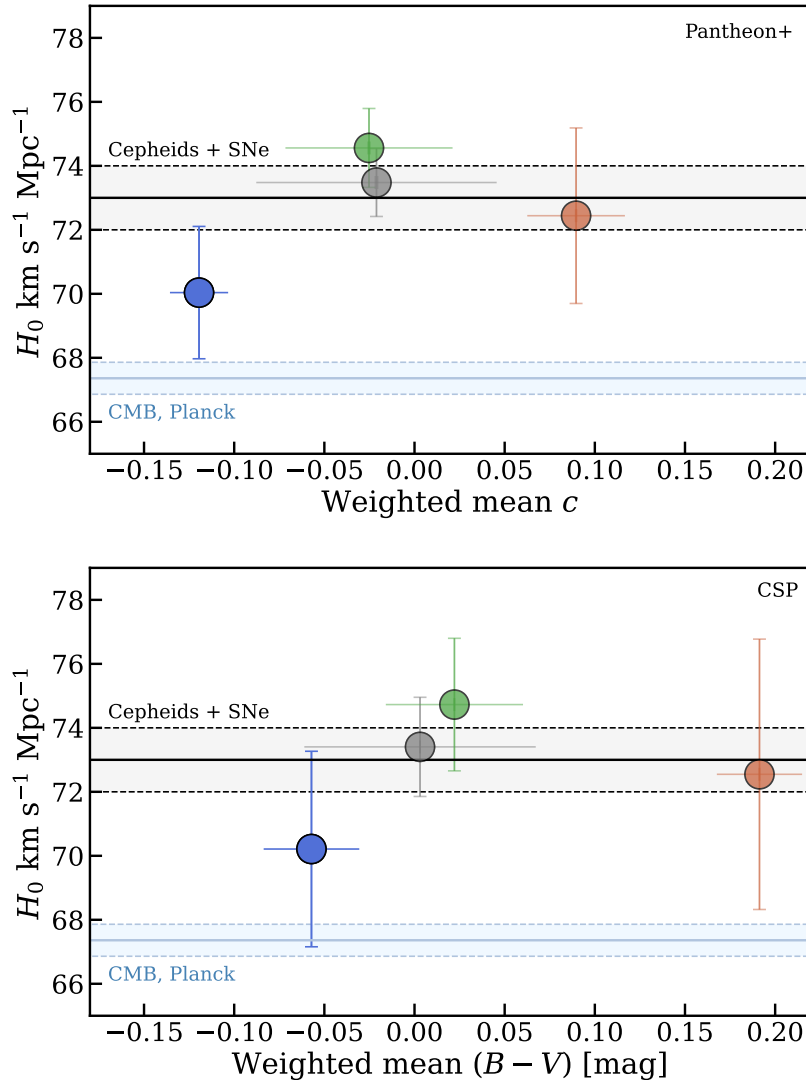


Figure 2. H_0 as a function of color. *Upper panel:* shows H_0 for Pantheon+. *Lower panel:* shows H_0 for CSP. Blue, green and red symbols mark the color range of the three color bins as defined in Table 1. The grey symbols refer to the measurement using all data. The weighted mean quantity (i.e., color) is shown with the weighted standard deviation to represent the scatter of the quantity instead of the error of the weighted mean, which is $< 0.1\%$.

ent data compilation, lightcurve fitter, and SN Ia color definition as described for CSP, a similar H_0 trend as shown in the lower panel of Figure 2 is obtained, with the lowest H_0 value of $70.3 \pm 3.0 \text{ km s}^{-1} \text{Mpc}^{-1}$ for blue SNe. All H_0 values for blue SNe Ia in comparison to the H_0 values for the entire data sets are summarized in Table 2. We note that a small difference between the best-fit H_0 from the Pantheon+ likelihood and the SHOES result reflects a difference in the corresponding likelihoods, which use distance moduli to the calibrators either as latent variables in a joint fit (SHOES) or as fixed values in modeling the supernova data (Pantheon+). In this paper we focus on blue SNe since we wish to explore the consequences of minimizing the effects of dust ex-

tinction. Nevertheless, we note that in both Pantheon+ and CSP samples, there is a downturn in H_0 for the reddest SNe (see Figure 2). This downturn is less significant and more complex in that it may or may not be due to effects related to dust extinction.

One of the caveats of such a color bin test may be the so-called ‘Eddington bias’ (Eddington 1913). An SN Ia with a color measurement falling on one side of the color cut with error bars extending into both color bins may, in reality, have a color that is either bluer or redder than the given color cut. This can introduce a bias in fitting the parameters, as also discussed in Kowalski et al. (2008) and Rubin et al. (2025). In Appendix B, we

Table 2. H_0 from blue SNe

	Pantheon+	CSP
Blue SNe Ia	70.0 (2.1)	70.3 (3.0)
All data	73.5 (1.1)	73.4 (1.5)

NOTE—Details of other H_0 values and model parameters are provided in Tables 3 and 4. Units: $\text{km s}^{-1} \text{Mpc}^{-1}$.

verify the effect by only considering SNe Ia with measured colors and uncertainties, which are fully included in a bin. We find that only a very small percentage of SNe Ia have color measurements with uncertainties extending into the neighboring color bin, which does not significantly alter our results. We acknowledge that this does not exclude a possible bias by SNe Ia that may have precisely but inaccurately measured lightcurve parameters. As discussed above, the choice of binning is aimed at identifying the bluest, least-extinguished SNe Ia. Alternative choices of binning are explored in Appendix A and B and shown in Appendix Figures 7, 8 and 10.

4. DISCUSSION

The H_0 trend with SN color may signal a dependency on the prescription for disentangling the SN Ia intrinsic color distribution and extrinsic color effects, and correcting for dust extinction. The differences in the response to dust models for the red SNe Ia (different approaches for Pantheon+ and CSP) appear to strengthen this suspicion. Thus, taken at face value, the two compilations (Pantheon+ and CSP) of blue SNe Ia yield similar H_0 values of $70.0 \pm 2.1 \text{ km s}^{-1} \text{Mpc}^{-1}$ and $70.3 \pm 3.0 \text{ km s}^{-1} \text{Mpc}^{-1}$, respectively, which is consistent with their uncertainties with the CMB value (but also consistent with the standard analysis of these data sets). In principle, the selected subsamples of blue or red SNe Ia may have different physical or environmental characteristics. We discuss a range of such possibilities below.

Alternatively, the H_0 dependency of SN color can be a statistical fluke and be dependent on the choice of binning due to the low number of SNe Ia in each bin. However, as we demonstrate in Appendix A, the H_0 dependency on color is reproduced with different choices of binning, and the inferred H_0 values appear to increase systematically with SN color up to $c \sim 0 \text{ mag}$ in both samples. The H_0 measurement obtained for the blue bin is a part of this systematic trend (see Sect. 4.4, Appendix A and B).

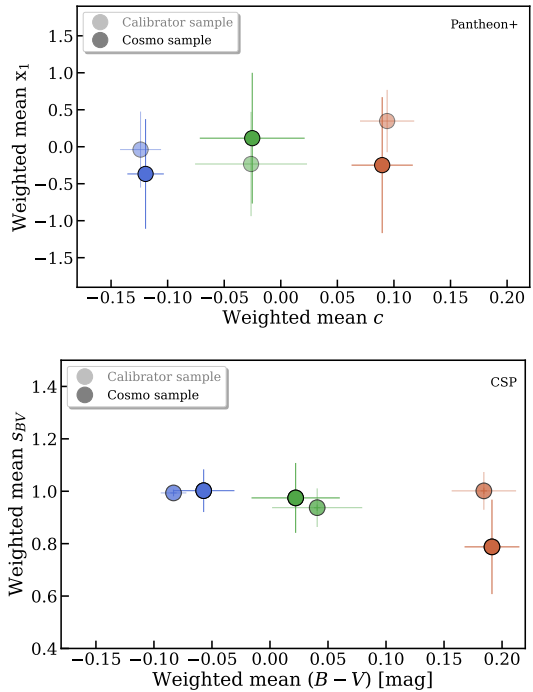


Figure 3. Lightcurve shape parameter for different SN Ia colors. *Upper panel:* shows x_1 for Pantheon+. *Lower panel:* shows s_{BV} for CSP. Shown are the weighted standard deviations to represent the scatter of the quantities in each bin. The errors in the mean are smaller than the symbol sizes.

4.1. What are Blue SNe Ia?

The empirical luminosity-color and luminosity-decline rate relations imply that intrinsically brighter SNe Ia are bluer and have slower declining lightcurves (Phillips 1993; Tripp 1998). Indeed, some of the brightest SNe Ia, 91T-like SNe (Filippenko et al. 1992; Phillips et al. 1992) are found to have blue colors (Stritzinger et al. 2018). For the majority of ‘normal-bright’ and ‘normal-declining’ SNe Ia, the colors at peak brightness are similar, with theoretical models able to produce SNe Ia with blue colors (Hoeflich et al. 2017). However, as long as the distribution of lightcurve shape parameters is the same in the different bins, this should not lead to differences in the inferred H_0 .

Figure 3 shows that the SNe Ia in the blue bin in the Pantheon+ sample have a weighted mean SALT2 lightcurve shape parameter consistent within their uncertainties with that of SNe Ia in the green and red bins. This is valid for both the calibration and the HF SN Ia sample. The CSP SNe Ia in the red bin appear to have slightly lower s_{BV} . There is no obvious trend, but if anything, they are opposite in the two cases. Thus, there is no indication of clear differences among the three bins, in either sample, and we conclude that the lower H_0

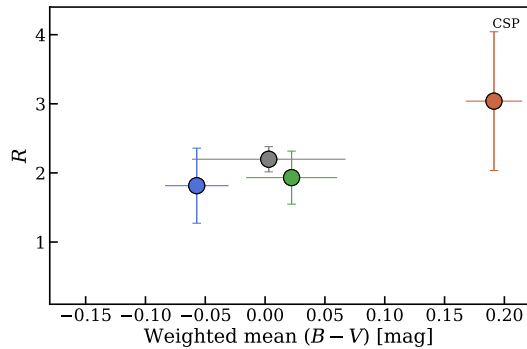


Figure 4. Color correction parameter for different SN Ia colors. Here, R for the CSP sample obtained for the blue, green, and red bins, including R when using all data (gray symbol). The weighted standard deviations are shown to represent the scatter of color in each bin. The errors in the mean are smaller than the symbol sizes.

for blue SNe Ia is unlikely due to lightcurve differences among the bins.

For unextinguished SNe Ia, the color correction parameters, β or R , reduce to a correction coefficient of the intrinsic luminosity-color relation. Thus, a dependence of the local slope on SN Ia color may be expected if dust extinction has not been correctly accounted for (Mandel et al. 2017).

Indeed, smaller values of β have been obtained for bluer SNe Ia than for redder SNe Ia (Amanullah et al. 2010; González-Gaitán et al. 2021), with values of β typically $\lesssim 2.6$ (although see Rose et al. 2022, for very red supernovae). Such small β values are unlikely due to dust alone ($R_V \approx \beta - 1.0$), as such steep extinction curves ($R_V \lesssim 2$) are inconsistent with observed dust properties in the ISM of galaxies (see Sect. 1). For Pantheon+, β as a function of SN color is accounted for by the employed color model, which is trained on SNe Ia at $z > 0.03$ and adopted for the calibration sample. However, for CSP, we can test if R , which can be interpreted similarly to β , changes with SN color. Figure 4 shows R as a function of color. Indeed, we see the expected trend of R values increasing with color as SNe Ia become redder and hence more reddened.

Figures 3 and 4 are therefore consistent with bluer supernovae being less reddened. We conclude that SNe Ia with $c < -0.1$ (blue bin) in Pantheon+ likely are dominated by SNe Ia close to their intrinsic peak magnitudes and colors. Consequently, SNe Ia with measured $c > -0.1$, must be more strongly affected by dust (Wojtak et al. 2023; Wojtak & Hjorth 2024; Popovic et al. 2024b; Vincenzi et al. 2024).

4.2. Blue SNe Ia and their Locations in Galaxies

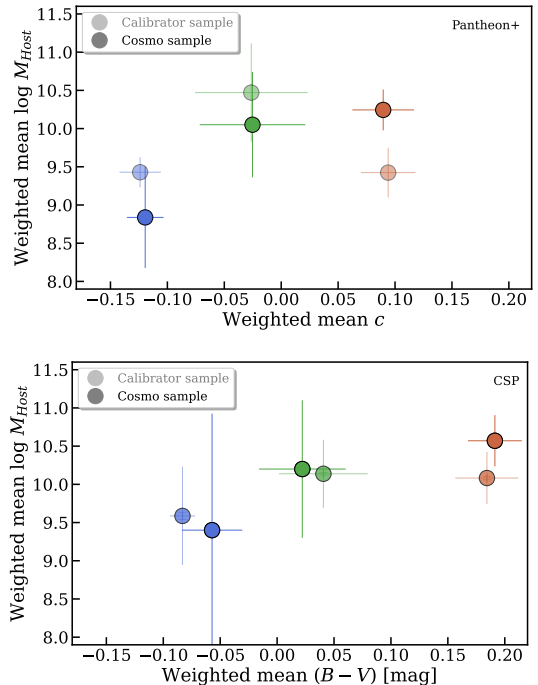


Figure 5. Host-galaxy mass distribution with color. *Upper panel:* shows $\log M_{\text{host}}$ for the Pantheon+ data compilation. Host-galaxy masses are taken from the online tables of both data compilations (Sect. 2). We note that host-galaxy masses are not available for all hosts of the Pantheon+ data compilation. The fractions of host galaxies with measurements for SNe Ia in the calibration sample are 0.3 (blue), 0.64 (green), and 0.64 (red), and for SNe Ia in the cosmological sample are 0.8 (blue), 0.93 (green), and 0.97 (red). Shown are the weighted standard deviations to represent the scatter of the quantities in each bin. The errors in the mean are smaller than the symbol sizes. *Lower panel:* shows $\log M_{\text{host}}$ for CSP.

The majority of normal-bright and normal-declining SNe Ia with both blue and red colors occur in late-type galaxies. This is the case for a subsample of the Pantheon+ SNe Ia (Pruzhinskaya et al. 2020), and all SNe Ia with Cepheid distances (Riess et al. 2016, 2022a). Typically, late-type galaxies are gas- and dust-rich spirals with ongoing star formation (Kennicutt 1983).

Early-type galaxies also host normal SNe Ia, including the so-called ‘transitional’ SNe Ia. These events decline faster than the standard normal SNe Ia but are not as faint as SN 1991bg-like SNe Ia (Taubenberger et al. 2008; Gall et al. 2018; Harvey et al. 2023). These SNe Ia have $B - V$ color curves that are those of normal SNe Ia alike, but some such transitional SNe Ia can have blue colors at peak brightness (e.g., Sahu et al. 2013; Gall et al. 2018; Izzo et al. 2026). Interestingly, galaxies with SBF distances are primarily early-type galaxies (Khetan et al. 2021; Jensen et al. 2021).

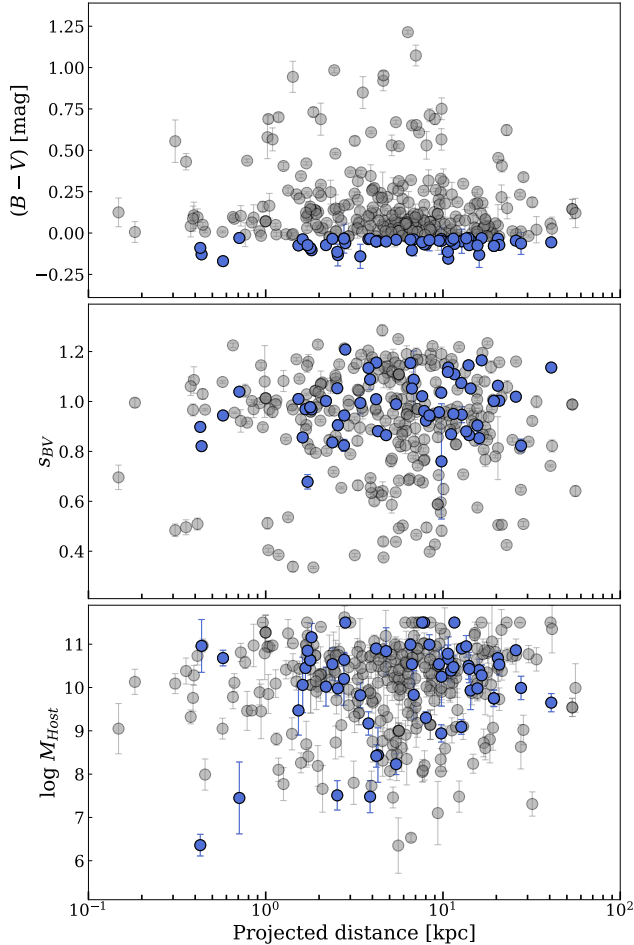


Figure 6. Projected distance of SNe Ia in CSP. Highlighted in blue are SNe Ia in the blue color bin ($B - V < -0.03$ mag). *Upper panel:* SN Ia color. *Middle panel:* light curve shape parameter. *Lower panel:* host-galaxy mass.

Studies of SN Ia samples show that SNe Ia in both early- and late-type galaxies have, on average, a similar SN Ia color distribution (e.g., mean SALT $c \sim 0$), although SNe Ia in early-type galaxies appear to be marginally bluer (Sullivan et al. 2010; Henne et al. 2017; Pruzhinskaya et al. 2020). After lightcurve shape and color corrections, SNe Ia in early-type galaxies, or galaxies with low specific star formation rates, high stellar masses, and high metallicity, are found to be brighter than those in late-type galaxies (Gallagher et al. 2008; Hicken et al. 2009a; Sullivan et al. 2010; Kelly et al. 2010; Khetan et al. 2021). Other recent works show that by splitting the SN Ia sample of the 5-year Dark Energy Survey into two color bins with $c < 0$ and $c > 0$, a lower r.m.s. scatter in the Hubble residuals can be achieved for SNe Ia in the bluer bin, which are also hosted in less massive and blue $U - R$ colored galaxies (Kelsey et al. 2023).

Figure 5 shows that Pantheon+ SNe Ia in the blue bin appear to have less massive hosts than SNe Ia in the redder bin, although there are only a few SNe Ia with host-galaxy mass measurements. For massive galaxies, there is a positive correlation between extinction and star-formation rate. However, for less massive galaxies ($< 10^{10}$ solar masses), Zahid et al. (2013) found that extinction is anticorrelated with star-formation rate. Thus, one can achieve low extinction for low-mass, star-forming galaxies, consistent with blue SNe being located in low-extinction environments.

Moreover, we calculate the projected distances of the CSP SNe Ia as in Uddin et al. (2024). As shown in Figure 6, there is no obvious preference for the projected distance of blue SNe Ia relative to redder SNe Ia, although this does not imply that blue SNe Ia are at the same location as redder SNe Ia, e.g., close to the center of galaxies. Indeed, Pritchett et al. (2024) show that SNe Ia with SALT2 $c < 0$ mag are missing in the inner regions of disk-dominated galaxies, which are home to SNe Ia with $c > 0$ mag. While a link between the SN Ia age and the age difference between the disk and bulge is ruled out as the origin of the missing blue SNe Ia, significant dust extinction in the inner region of the disk is likely to redden the SNe Ia. Since SNe with SALT2 $c < -0.1$ mag are unlikely to be strongly affected by extinction, the sight lines towards blue SNe must largely be dust free, independent of their projected distance. We suggest that blue, nearly unextinguished SNe Ia are likely located in the outskirts and halos of galaxies where dust column densities can be low.

4.3. Complexity of Dust Extinction

Figure 2 and Appendix Figures 7, 8 and 9 show that independent of data sets, dust models, and lightcurve fitters, ‘red’ SNe ($c > -0.1$, $(B - V) > 0.015$ mag) lead to high H_0 values consistent with Riess et al. (2022a) Phillips et al. (2026) within uncertainties. Since red SNe Ia are either red and faint intrinsically or they are brighter and bluer SNe Ia that are affected by dust extinction, unaccounted-for systematics of both color effects are plausible reasons for the H_0 variations. As shown by Wojtak & Hjorth (2022), simply accounting for different β for the calibration and the cosmological sample leads to smaller values of H_0 than favored in the literature using a global β . Wojtak & Hjorth (2022) found that β appears to be larger for SNe in the calibration sample than the SNe in the cosmological sample. This points to either differences in dust extinction of SNe Ia in the two samples, or differences in the intrinsic color distribution of SN Ia in each of the samples. While this could be the result of an incorrect dust cor-

rection method (Scolnic et al. 2015), the H_0 variations with SN Ia color noticed in both Pantheon+ and CSP (see Figure 2) suggest that the full complexity of dust extinction of SNe Ia may not be captured by any of the dust models employed in lightcurve fitters and cosmological models.

Indeed, recent 3D Milky Way R_V mapping reveals complex patterns throughout the different ISM regions, with large (> 3.1) R_V values found in both high and low density ISM regions, surprisingly low R_V values in moderate density regions, and a strong correlation between high R_V values and star formation (Zhang & Green 2025). Measurements of reddening curves through single-cloud and translucent cloud sight lines of the diffuse ISM of the Milky Way result in $R_V = 3.1 \pm 0.4$ (Fitzpatrick et al. 2019; Siebenmorgen et al. 2023), in agreement with the mean R_V value of the Milky Way. On the other hand, $R_V > 3.1$ are typically found through sight lines of the dense and cold ISM (e.g., Fitzpatrick et al. 2019). In some such single-cloud sight lines, and strongly star forming regions in the Large Magellanic Cloud bar, a large ‘dark dust’ component of up to 1–3 mag has been found (De Marchi et al. 2020; Siebenmorgen et al. 2020; De Marchi et al. 2021). Dark dust, also known as gray dust, is wavelength-independent dust originating from very large grains. Such dust leads to flat extinction curves that do not affect the colors of an extinguished object but affect the brightness of the object, and can add further complexity to dust extinction corrections of SN Ia.

While the majority of host-galaxy sight lines toward SNe Ia are likely a combination of different ISM regions, possibly resulting in average R_V values (Siebenmorgen et al. 2020, 2023), some sight lines may be dominated by a certain ISM region, ISM density, or dust composition with very individual R_V values. Given this inhomogeneous and complex nature of dust along the line of sight to SN Ia and that SNe Ia do not have a preferred location in galaxies, employing global host-galaxy (e.g., extinction, mass) corrections is likely to lead to under- or over-estimations of extinction, and hence SN Ia magnitudes and colors.

4.4. Low Number Statistics

The H_0 values measured from SNe Ia in the blue bin can be argued to be a statistical fluctuation. This is, because the number of calibrating and HF SNe Ia (see Table 1) in the blue bin is low. However, the calibrating-to-HF SNe Ia ratio in the blue bin is comparable to, if not larger than, the calibrating-to-HF SNe Ia ratio of the entire sample (e.g., Pantheon+ blue bin). The same is the case for the green and red bins (see Table 1).

Hence, we tested this possibility in Appendix A, where we split the Pantheon+ sample into six color bins with a constant $\Delta c = 0.053$ mag. Each color bin has a similar number of SNe Ia as the blue bin. It is expected that H_0 values derived from these bins would fluctuate randomly around a mean value. Figure 7 shows that this is not the case. Rather, there is a gradual increase of H_0 with color, reaching a high H_0 value > 76 km s⁻¹ Mpc⁻¹ around $\bar{c} \approx 0$ mag. As also shown in Wojtak & Hjorth (2024, Figure 1) and noticed in Figure 5, such high H_0 values are driven by SNe Ia in high-stellar-mass host galaxies ($M_\star > 10^{10} M_\odot$), for which dust extinction is likely underestimated for reddened SNe Ia. We also tested this for the CSP sample, which is split into four color bins with $\Delta(B-V) = 0.08$ mag (Appendix B) and find a similar trend of H_0 with color, i.e., an increase of H_0 from blue toward redder SNe Ia and a decrease of H_0 at the reddest end, rather than random fluctuations.

We note that while statistical fluctuation causing the low H_0 may be unlikely, H_0 is nevertheless sensitive to the low number of SNe Ia, their lightcurve parameter estimations, and extinction corrections. The latter may be affected by possibly only a few, unextinguished SNe Ia in the lightcurve fitter (e.g., SALT2) training samples. With upcoming major transient surveys on the horizon, such as the Vera C. Rubin Observatory Legacy Survey of Space and Time and other simultaneous, complementary photometric and spectroscopic surveys, the number of blue, nearly unextinguished SNe Ia will increase. This will allow a robust measurement of H_0 derived entirely from blue SNe Ia and thus, independent of dust corrections.

5. CONCLUSION

In this paper, we used different SN Ia data sets for which SN Ia lightcurve parameters, such as lightcurve shape and color parameters, have been obtained with different lightcurve fitting methods (SALT2 and SNooPy). We used data compilations from Pantheon+ and CSP (Brout et al. 2022a,b; Scolnic et al. 2022; Uddin et al. 2024) together with Cepheid distances (Riess et al. 2022b).

The key findings are summarized below:

- Independent of the data set, lightcurve fitter, and cosmological model investigated here, we find low H_0 values (~ 70 km s⁻¹ Mpc⁻¹) for nearly unextinguished blue SNe Ia.
- SNe Ia with colors $c > -0.1$ mag tend to result in higher H_0 values ($H_0 > 72$ km s⁻¹ Mpc⁻¹).
- The H_0 values from nearly unextinguished blue SNe Ia are within 1.2σ of H_0 values from extin-

guished SNe Ia (green bin) and within 1σ of those measured from the CMB. This is a net effect of (i) a smaller best-fit value ($\sim 3 \text{ km s}^{-1} \text{ Mpc}^{-1}$) and (ii) larger errors due to smaller sample size. We stress that our results (see Figure 2) are fully consistent with previously published results of high H_0 values from the same data (Riess et al. 2022a; Uddin et al. 2024). The errors on our H_0 values from the blue (and red) SNe Ia encompass this 'high' value of H_0 . At the same time, the lower mean H_0 value and the larger error associated with it are also consistent with a 'low' H_0 value.

- There seems to be no obvious difference of the projected distance of blue SNe Ia compared to redder SNe Ia although blue SNe Ia must be located in low-extinction environments.

Our findings suggest that the majority of SNe Ia in cosmological samples may be affected by more complex dust extinction than what is captured by dust models currently employed in the standardization of SNe Ia and cosmological models. As directly measuring extinction

for each SNe Ia in distant galaxies is challenging, turning to only blue, presumably unextinguished, SNe Ia may be a promising path for future cosmology. Including reddened supernovae requires careful modeling of SNe Ia populations in relation to their environments. Along these lines, recent improvements in matching SNe Ia in the Hubble flow against the calibration SNe Ia resulted in as low values of the Hubble constant as the estimate obtained in this study from blue SNe Ia (Wojtak & Hjorth 2025b; Martins et al. 2025).

- 1 This work is supported by a VILLUM FONDEN Young
- 2 Investigator Grant (project No. 25501), a Villum Ex-
- 3 periment grant (VIL69896), and by research grants
- 4 (VIL16599, VIL54489) from VILLUM FONDEN. We
- 5 thank the anonymous referee for constructive comments,
- 6 and we thank Stephen Thorp, Gautham Narayan, and
- 7 Chris Burns for helpful discussions.

Software: `astropy` (Astropy Collaboration et al. 2013; Collaboration et al. 2022), `emcee` (Foreman-Mackey et al. 2013)

REFERENCES

- Amanullah, R., Lidman, C., Rubin, D., et al. 2010, *ApJ*, 716, 712, doi: [10.1088/0004-637X/716/1/712](https://doi.org/10.1088/0004-637X/716/1/712)
- Amanullah, R., Goobar, A., Johansson, J., et al. 2014, *ApJL*, 788, L21, doi: [10.1088/2041-8205/788/2/L21](https://doi.org/10.1088/2041-8205/788/2/L21)
- Ashall, C., Mazzali, P. A., Stritzinger, M. D., et al. 2018, *MNRAS*, 477, 153, doi: [10.1093/mnras/sty632](https://doi.org/10.1093/mnras/sty632)
- Astropy Collaboration, Robitaille, T. P., Tollerud, E. J., et al. 2013, *A&A*, 558, A33, doi: [10.1051/0004-6361/201322068](https://doi.org/10.1051/0004-6361/201322068)
- Betoule, M., Kessler, R., Guy, J., et al. 2014, *A&A*, 568, A22, doi: [10.1051/0004-6361/201423413](https://doi.org/10.1051/0004-6361/201423413)
- Blakeslee, J. P., Jensen, J. B., Ma, C.-P., Milne, P. A., & Greene, J. E. 2021, *ApJ*, 911, 65, doi: [10.3847/1538-4357/abe86a](https://doi.org/10.3847/1538-4357/abe86a)
- Brout, D., & Scolnic, D. 2021, *ApJ*, 909, 26, doi: [10.3847/1538-4357/abd69b](https://doi.org/10.3847/1538-4357/abd69b)
- Brout, D., Scolnic, D., Kessler, R., et al. 2019, *ApJ*, 874, 150, doi: [10.3847/1538-4357/ab08a010.48550/arXiv.1811.02377](https://doi.org/10.3847/1538-4357/ab08a010.48550/arXiv.1811.02377)
- Brout, D., Scolnic, D., Popovic, B., et al. 2022a, *ApJ*, 938, 110, doi: [10.3847/1538-4357/ac8e04](https://doi.org/10.3847/1538-4357/ac8e04)
- Brout, D., Taylor, G., Scolnic, D., et al. 2022b, *ApJ*, 938, 111, doi: [10.3847/1538-4357/ac8bcc](https://doi.org/10.3847/1538-4357/ac8bcc)
- Bulla, M., Goobar, A., & Dhawan, S. 2018, *MNRAS*, 479, 3663, doi: [10.1093/mnras/sty1619](https://doi.org/10.1093/mnras/sty1619)
- Burns, C. R., Stritzinger, M., Phillips, M. M., et al. 2011, *AJ*, 141, 19, doi: [10.1088/0004-6256/141/1/19](https://doi.org/10.1088/0004-6256/141/1/19)
- . 2014, *ApJ*, 789, 32, doi: [10.1088/0004-637X/789/1/32](https://doi.org/10.1088/0004-637X/789/1/32)
- Burns, C. R., Parent, E., Phillips, M. M., et al. 2018, *ApJ*, 869, 56, doi: [10.3847/1538-4357/aae51c10.48550/arXiv.1809.06381](https://doi.org/10.3847/1538-4357/aae51c10.48550/arXiv.1809.06381)
- Calabrese, E., Hill, J. C., Jense, H. T., et al. 2025, *JCAP*, 2025, 063, doi: [10.1088/1475-7516/2025/11/063](https://doi.org/10.1088/1475-7516/2025/11/063)
- Calzetti, D., Kinney, A. L., & Storchi-Bergmann, T. 1994, *ApJ*, 429, 582, doi: [10.1086/174346](https://doi.org/10.1086/174346)
- Cardelli, J. A., Clayton, G. C., & Mathis, J. S. 1989, *ApJ*, 345, 245, doi: [10.1086/167900](https://doi.org/10.1086/167900)
- Collaboration, T. A., Price-Whelan, A. M., Lim, P. L., et al. 2022, *The Astrophysical Journal*, 935, 167, doi: [10.3847/1538-4357/ac7c74](https://doi.org/10.3847/1538-4357/ac7c74)
- Contreras, C., Hamuy, M., Phillips, M. M., et al. 2010, *AJ*, 139, 519, doi: [10.1088/0004-6256/139/2/519](https://doi.org/10.1088/0004-6256/139/2/519)
- Dainotti, M. G., De Simone, B., Schiavone, T., et al. 2021, *ApJ*, 912, 150, doi: [10.3847/1538-4357/abeb73](https://doi.org/10.3847/1538-4357/abeb73)
- Dainotti, M. G., De Simone, B. D., Schiavone, T., et al. 2022, *Galaxies*, 10, 24, doi: [10.3390/galaxies10010024](https://doi.org/10.3390/galaxies10010024)
- Dainotti, M. G., De Simone, B., Garg, A., et al. 2025, *Journal of High Energy Astrophysics*, 48, 100405, doi: [10.1016/j.jheap.2025.100405](https://doi.org/10.1016/j.jheap.2025.100405)
- De Marchi, G., Panagia, N., & Milone, A. P. 2020, *ApJ*, 899, 114, doi: [10.3847/1538-4357/aba834](https://doi.org/10.3847/1538-4357/aba834)

- . 2021, *ApJ*, 922, 135, doi: [10.3847/1538-4357/ac2a28](https://doi.org/10.3847/1538-4357/ac2a28)
- Dhawan, S., Thorp, S., Mandel, K. S., et al. 2023, *MNRAS*, 524, 235, doi: [10.1093/mnras/stad1590](https://doi.org/10.1093/mnras/stad1590)
- Di Valentino, E., Mena, O., Pan, S., et al. 2021, *Classical and Quantum Gravity*, 38, 153001, doi: [10.1088/1361-6382/ac086d](https://doi.org/10.1088/1361-6382/ac086d)
- Draine, B. T. 2011, *Physics of the Interstellar and Intergalactic Medium* (Princeton University Press)
- Eddington, A. S. 1913, *MNRAS*, 73, 359, doi: [10.1093/mnras/73.5.359](https://doi.org/10.1093/mnras/73.5.359)
- Elias-Rosa, N., Benetti, S., Cappellaro, E., et al. 2006, *MNRAS*, 369, 1880, doi: [10.1111/j.1365-2966.2006.10430.x](https://doi.org/10.1111/j.1365-2966.2006.10430.x)
- Elias-Rosa, N., Benetti, S., Turatto, M., et al. 2008, *MNRAS*, 384, 107, doi: [10.1111/j.1365-2966.2007.12638.x](https://doi.org/10.1111/j.1365-2966.2007.12638.x)
- Filippenko, A. V., Richmond, M. W., Matheson, T., et al. 1992, *ApJL*, 384, L15, doi: [10.1086/186252](https://doi.org/10.1086/186252)
- Fitzpatrick, E. L. 1999, *PASP*, 111, 63, doi: [10.1086/316293](https://doi.org/10.1086/316293)
- Fitzpatrick, E. L., Massa, D., Gordon, K. D., Bohlin, R., & Clayton, G. C. 2019, *ApJ*, 886, 108, doi: [10.3847/1538-4357/ab4c3a](https://doi.org/10.3847/1538-4357/ab4c3a)
- Folatelli, G., Phillips, M. M., Burns, C. R., et al. 2010, *AJ*, 139, 120, doi: [10.1088/0004-6256/139/1/120](https://doi.org/10.1088/0004-6256/139/1/120)
- Foreman-Mackey, D., Hogg, D. W., Lang, D., & Goodman, J. 2013, *PASP*, 125, 306, doi: [10.1086/670067](https://doi.org/10.1086/670067)
- Freedman, W. L. 2021, *ApJ*, 919, 16, doi: [10.3847/1538-4357/ac0e95](https://doi.org/10.3847/1538-4357/ac0e95)
- Freedman, W. L., Madore, B. F., Hoyt, T. J., et al. 2025, *ApJ*, 985, 203, doi: [10.3847/1538-4357/adce78](https://doi.org/10.3847/1538-4357/adce78)
- Freedman, W. L., Madore, B. F., Gibson, B. K., et al. 2001, *ApJ*, 553, 47, doi: [10.1086/32063810.48550/arXiv.astro-ph/0012376](https://doi.org/10.1086/32063810.48550/arXiv.astro-ph/0012376)
- Freedman, W. L., Madore, B. F., Hatt, D., et al. 2019, *ApJ*, 882, 34, doi: [10.3847/1538-4357/ab2f7310.48550/arXiv.1907.05922](https://doi.org/10.3847/1538-4357/ab2f7310.48550/arXiv.1907.05922)
- Galbany, L., de Jaeger, T., Riess, A. G., et al. 2023, *A&A*, 679, A95, doi: [10.1051/0004-6361/202244893](https://doi.org/10.1051/0004-6361/202244893)
- Gall, C., Stritzinger, M. D., Ashall, C., et al. 2018, *A&A*, 611, A58, doi: [10.1051/0004-6361/201730886](https://doi.org/10.1051/0004-6361/201730886)
- Gallagher, J. S., Garnavich, P. M., Caldwell, N., et al. 2008, *ApJ*, 685, 752, doi: [10.1086/590659](https://doi.org/10.1086/590659)
- Garnavich, P., Wood, C. M., Milne, P., et al. 2023, *ApJ*, 953, 35, doi: [10.3847/1538-4357/ace04b](https://doi.org/10.3847/1538-4357/ace04b)
- González-Gaitán, S., de Jaeger, T., Galbany, L., et al. 2021, *MNRAS*, 508, 4656, doi: [10.1093/mnras/stab2802](https://doi.org/10.1093/mnras/stab2802)
- Goobar, A. 2008, *ApJL*, 686, L103, doi: [10.1086/593060](https://doi.org/10.1086/593060)
- Grayling, M., Thorp, S., Mandel, K. S., et al. 2024, *MNRAS*, 531, 953, doi: [10.1093/mnras/stae1202](https://doi.org/10.1093/mnras/stae1202)
- Guillochon, J., Parrent, J., Kelley, L. Z., & Margutti, R. 2017, *ApJ*, 835, 64, doi: [10.3847/1538-4357/835/1/64](https://doi.org/10.3847/1538-4357/835/1/64)
- Guy, J., Astier, P., Nobili, S., Regnault, N., & Pain, R. 2005, *A&A*, 443, 781, doi: [10.1051/0004-6361:20053025](https://doi.org/10.1051/0004-6361:20053025)
- Guy, J., Astier, P., Baumont, S., et al. 2007, *A&A*, 466, 11, doi: [10.1051/0004-6361:20066930](https://doi.org/10.1051/0004-6361:20066930)
- Guy, J., Sullivan, M., Conley, A., et al. 2010, *A&A*, 523, A7, doi: [10.1051/0004-6361/201014468](https://doi.org/10.1051/0004-6361/201014468)
- Harvey, L., Maguire, K., Magee, M. R., et al. 2023, *MNRAS*, 522, 4444, doi: [10.1093/mnras/stad1226](https://doi.org/10.1093/mnras/stad1226)
- Henne, V., Pruzhinskaya, M. V., Rosnet, P., et al. 2017, *NewA*, 51, 43, doi: [10.1016/j.newast.2016.08.009](https://doi.org/10.1016/j.newast.2016.08.009)
- Hicken, M., Wood-Vasey, W. M., Blondin, S., et al. 2009a, *ApJ*, 700, 1097, doi: [10.1088/0004-637X/700/2/1097](https://doi.org/10.1088/0004-637X/700/2/1097)
- Hicken, M., Challis, P., Jha, S., et al. 2009b, *ApJ*, 700, 331, doi: [10.1088/0004-637X/700/1/331](https://doi.org/10.1088/0004-637X/700/1/331)
- Hicken, M., Challis, P., Kirshner, R. P., et al. 2012, *ApJS*, 200, 12, doi: [10.1088/0067-0049/200/2/12](https://doi.org/10.1088/0067-0049/200/2/12)
- Hoeflich, P., Hsiao, E. Y., Ashall, C., et al. 2017, *ApJ*, 846, 58, doi: [10.3847/1538-4357/aa84b2](https://doi.org/10.3847/1538-4357/aa84b2)
- Hubble, E. 1929, *Proceedings of the National Academy of Science*, 15, 168, doi: [10.1073/pnas.15.3.168](https://doi.org/10.1073/pnas.15.3.168)
- Izzo, L., Gall, C., Khetan, N., et al. 2026, *A&A*, 706, A381, doi: [10.1051/0004-6361/202556425](https://doi.org/10.1051/0004-6361/202556425)
- Jensen, J. B., Blakeslee, J. P., Ma, C.-P., et al. 2021, *ApJS*, 255, 21, doi: [10.3847/1538-4365/ac01e7](https://doi.org/10.3847/1538-4365/ac01e7)
- Jha, S., Riess, A. G., & Kirshner, R. P. 2007, *ApJ*, 659, 122, doi: [10.1086/512054](https://doi.org/10.1086/512054)
- Jha, S., Kirshner, R. P., Challis, P., et al. 2006, *AJ*, 131, 527, doi: [10.1086/497989](https://doi.org/10.1086/497989)
- Keel, W. C., Manning, A. M., Holwerda, B. W., Lintott, C. J., & Schawinski, K. 2014, *AJ*, 147, 44, doi: [10.1088/0004-6256/147/2/44](https://doi.org/10.1088/0004-6256/147/2/44)
- Kelly, P. L., Hicken, M., Burke, D. L., Mandel, K. S., & Kirshner, R. P. 2010, *ApJ*, 715, 743, doi: [10.1088/0004-637X/715/2/74310.48550/arXiv.0912.0929](https://doi.org/10.1088/0004-637X/715/2/74310.48550/arXiv.0912.0929)
- Kelsey, L., Sullivan, M., Smith, M., et al. 2021, *MNRAS*, 501, 4861, doi: [10.1093/mnras/staa3924](https://doi.org/10.1093/mnras/staa3924)
- Kelsey, L., Sullivan, M., Wiseman, P., et al. 2023, *MNRAS*, 519, 3046, doi: [10.1093/mnras/stac3711](https://doi.org/10.1093/mnras/stac3711)
- Kennicutt, R. C., J. 1983, *ApJ*, 272, 54, doi: [10.1086/161261](https://doi.org/10.1086/161261)
- Khetan, N., Izzo, L., Branchesi, M., et al. 2021, *A&A*, 647, A72, doi: [10.1051/0004-6361/202039196](https://doi.org/10.1051/0004-6361/202039196)
- Kowalski, M., Rubin, D., Aldering, G., et al. 2008, *ApJ*, 686, 749, doi: [10.1086/589937](https://doi.org/10.1086/589937)
- Krisciunas, K., Contreras, C., Burns, C. R., et al. 2017, *AJ*, 154, 211, doi: [10.3847/1538-3881/aa8df0](https://doi.org/10.3847/1538-3881/aa8df0)
- Leavitt, H. S., & Pickering, E. C. 1912, *Harvard College Observatory Circular*, 173, 1

- Lee, A. J., Freedman, W. L., Jang, I. S., Madore, B. F., & Owens, K. A. 2024, *ApJ*, 961, 132, doi: [10.3847/1538-4357/ad12c7](https://doi.org/10.3847/1538-4357/ad12c7)
- Lemaître, G. 1927, *Annales de la Société Scientifique de Bruxelles*, 47, 49
- Madore, B. F., & Freedman, W. L. 1995, *AJ*, 109, 1645, doi: [10.1086/117391](https://doi.org/10.1086/117391)
- Mandel, K. S., Narayan, G., & Kirshner, R. P. 2011, *ApJ*, 731, 120, doi: [10.1088/0004-637X/731/2/120](https://doi.org/10.1088/0004-637X/731/2/120)
- Mandel, K. S., Scolnic, D. M., Shariff, H., Foley, R. J., & Kirshner, R. P. 2017, *ApJ*, 842, 93, doi: [10.3847/1538-4357/aa6038](https://doi.org/10.3847/1538-4357/aa6038)
- Mandel, K. S., Thorp, S., Narayan, G., Friedman, A. S., & Avelino, A. 2022, *MNRAS*, 510, 3939, doi: [10.1093/mnras/stab3496](https://doi.org/10.1093/mnras/stab3496)
- Mandel, K. S., Wood-Vasey, W. M., Friedman, A. S., & Kirshner, R. P. 2009, *ApJ*, 704, 629, doi: [10.1088/0004-637X/704/1/629](https://doi.org/10.1088/0004-637X/704/1/629)
- Martins, G., González-Gaitán, S., Duarte, J., & Mourão, A. M. 2025, arXiv e-prints, arXiv:2511.14332, doi: [10.48550/arXiv.2511.14332](https://doi.org/10.48550/arXiv.2511.14332)
- Meldorf, C., Palmese, A., Brout, D., et al. 2023, *MNRAS*, 518, 1985, doi: [10.1093/mnras/stac3056](https://doi.org/10.1093/mnras/stac3056)
- Möller, A., Smith, M., Sako, M., et al. 2022, *MNRAS*, 514, 5159, doi: [10.1093/mnras/stac169110.48550/arXiv.2201.11142](https://doi.org/10.1093/mnras/stac169110.48550/arXiv.2201.11142)
- Moré, J. J. 1978, *Lecture Notes in Mathematics*, 630, 105
- Murakami, Y. S., Riess, A. G., Ferguson, H. C., et al. 2025, arXiv e-prints, arXiv:2503.09702, doi: [10.48550/arXiv.2503.09702](https://doi.org/10.48550/arXiv.2503.09702)
- Perlmutter, S., Aldering, G., Goldhaber, G., et al. 1999, *ApJ*, 517, 565, doi: [10.1086/307221](https://doi.org/10.1086/307221)
- Phillips, M. M. 1993, *ApJL*, 413, L105, doi: [10.1086/186970](https://doi.org/10.1086/186970)
- Phillips, M. M., Lira, P., Suntzeff, N. B., et al. 1999, *AJ*, 118, 1766, doi: [10.1086/301032](https://doi.org/10.1086/301032)
- Phillips, M. M., Wells, L. A., Suntzeff, N. B., et al. 1992, *AJ*, 103, 1632, doi: [10.1086/116177](https://doi.org/10.1086/116177)
- Phillips, M. M., Contreras, C., Hsiao, E. Y., et al. 2019, *PASP*, 131, 014001, doi: [10.1088/1538-3873/aae8bd](https://doi.org/10.1088/1538-3873/aae8bd)
- Phillips, M. M., Uddin, S. A., Burns, C. R., et al. 2026, *ApJ*, 998, 101, doi: [10.3847/1538-4357/ae2fef](https://doi.org/10.3847/1538-4357/ae2fef)
- Pietrzyński, G., Graczyk, D., Gallenne, A., et al. 2019, *Nature*, 567, 200, doi: [10.1038/s41586-019-0999-4](https://doi.org/10.1038/s41586-019-0999-4)
- Planck Collaboration, Aghanim, N., Akrami, Y., et al. 2020, *A&A*, 641, A6, doi: [10.1051/0004-6361/201833910](https://doi.org/10.1051/0004-6361/201833910)
- Popovic, B., Brout, D., Kessler, R., & Scolnic, D. 2023, *ApJ*, 945, 84, doi: [10.3847/1538-4357/aca273](https://doi.org/10.3847/1538-4357/aca273)
- Popovic, B., Brout, D., Kessler, R., Scolnic, D., & Lu, L. 2021, *ApJ*, 913, 49, doi: [10.3847/1538-4357/abf14f](https://doi.org/10.3847/1538-4357/abf14f)
- Popovic, B., Rigault, M., Smith, M., et al. 2024a, arXiv e-prints, arXiv:2406.06215, doi: [10.48550/arXiv.2406.06215](https://doi.org/10.48550/arXiv.2406.06215)
- Popovic, B., Wiseman, P., Sullivan, M., et al. 2024b, *MNRAS*, 534, 2263, doi: [10.1093/mnras/stae2164](https://doi.org/10.1093/mnras/stae2164)
- Pritchett, C., Thanjavur, K., Bottrell, C., & Gao, Y. 2024, *AJ*, 167, 131, doi: [10.3847/1538-3881/ad234b](https://doi.org/10.3847/1538-3881/ad234b)
- Pruzhinskaya, M. V., Novinskaya, A. K., Pauna, N., & Rosnet, P. 2020, *MNRAS*, 499, 5121, doi: [10.1093/mnras/staa3173](https://doi.org/10.1093/mnras/staa3173)
- Riess, A. G., Casertano, S., Yuan, W., et al. 2021, *ApJL*, 908, L6, doi: [10.3847/2041-8213/abdbaf](https://doi.org/10.3847/2041-8213/abdbaf)
- Riess, A. G., Press, W. H., & Kirshner, R. P. 1996, *ApJ*, 473, 88, doi: [10.1086/178129](https://doi.org/10.1086/178129)
- Riess, A. G., Filippenko, A. V., Challis, P., et al. 1998, *AJ*, 116, 1009, doi: [10.1086/300499](https://doi.org/10.1086/300499)
- Riess, A. G., Kirshner, R. P., Schmidt, B. P., et al. 1999, *AJ*, 117, 707, doi: [10.1086/300738](https://doi.org/10.1086/300738)
- Riess, A. G., Macri, L. M., Hoffmann, S. L., et al. 2016, *ApJ*, 826, 56, doi: [10.3847/0004-637X/826/1/56](https://doi.org/10.3847/0004-637X/826/1/56)
- Riess, A. G., Yuan, W., Macri, L. M., et al. 2022a, *ApJL*, 934, L7, doi: [10.3847/2041-8213/ac5c5b](https://doi.org/10.3847/2041-8213/ac5c5b)
- Riess, A. G., Breuval, L., Yuan, W., et al. 2022b, *ApJ*, 938, 36, doi: [10.3847/1538-4357/ac8f2410.48550/arXiv.2208.01045](https://doi.org/10.3847/1538-4357/ac8f2410.48550/arXiv.2208.01045)
- Rose, B. M., Popovic, B., Scolnic, D., & Brout, D. 2022, *MNRAS*, 516, 4822, doi: [10.1093/mnras/stac2500](https://doi.org/10.1093/mnras/stac2500)
- Rubin, D., Hoyt, T., Aldering, G., & Perlmutter, S. 2026, arXiv e-prints, arXiv:2601.19854, doi: [10.48550/arXiv.2601.19854](https://doi.org/10.48550/arXiv.2601.19854)
- Rubin, D., Aldering, G., Betoule, M., et al. 2025, *ApJ*, 986, 231, doi: [10.3847/1538-4357/adc0a5](https://doi.org/10.3847/1538-4357/adc0a5)
- Sahu, D. K., Anupama, G. C., & Anto, P. 2013, *MNRAS*, 430, 869, doi: [10.1093/mnras/sts609](https://doi.org/10.1093/mnras/sts609)
- Schlafly, E. F., Finkbeiner, D. P., Jurić, M., et al. 2012, *ApJ*, 756, 158, doi: [10.1088/0004-637X/756/2/158](https://doi.org/10.1088/0004-637X/756/2/158)
- Schlafly, E. F., Meisner, A. M., Stutz, A. M., et al. 2016, *ApJ*, 821, 78, doi: [10.3847/0004-637X/821/2/78](https://doi.org/10.3847/0004-637X/821/2/78)
- Schmidt, B. P., Suntzeff, N. B., Phillips, M. M., et al. 1998, *ApJ*, 507, 46, doi: [10.1086/306308](https://doi.org/10.1086/306308)
- Schombert, J., McGaugh, S., & Lelli, F. 2020, *AJ*, 160, 71, doi: [10.3847/1538-3881/ab9d88](https://doi.org/10.3847/1538-3881/ab9d88)
- Scolnic, D., & Kessler, R. 2016, *ApJL*, 822, L35, doi: [10.3847/2041-8205/822/2/L35](https://doi.org/10.3847/2041-8205/822/2/L35)
- Scolnic, D., Casertano, S., Riess, A., et al. 2015, *ApJ*, 815, 117, doi: [10.1088/0004-637X/815/2/117](https://doi.org/10.1088/0004-637X/815/2/117)
- Scolnic, D., Brout, D., Carr, A., et al. 2022, *ApJ*, 938, 113, doi: [10.3847/1538-4357/ac8b7a](https://doi.org/10.3847/1538-4357/ac8b7a)
- Scolnic, D., Riess, A. G., Murakami, Y. S., et al. 2025, *ApJL*, 979, L9, doi: [10.3847/2041-8213/ada0bd](https://doi.org/10.3847/2041-8213/ada0bd)

- Siebenmorgen, R., Krelowski, J., Smoker, J., Galazutdinov, G., & Bagnulo, S. 2020, *A&A*, 641, A35, doi: [10.1051/0004-6361/202037511](https://doi.org/10.1051/0004-6361/202037511)
- Siebenmorgen, R., Smoker, J., Krelowski, J., Gordon, K., & Chini, R. 2023, *A&A*, 676, A132, doi: [10.1051/0004-6361/202244594](https://doi.org/10.1051/0004-6361/202244594)
- Stritzinger, M. D., Phillips, M. M., Boldt, L. N., et al. 2011, *AJ*, 142, 156, doi: [10.1088/0004-6256/142/5/156](https://doi.org/10.1088/0004-6256/142/5/156)
- Stritzinger, M. D., Shappee, B. J., Piro, A. L., et al. 2018, *ApJL*, 864, L35, doi: [10.3847/2041-8213/aadd46](https://doi.org/10.3847/2041-8213/aadd46)
- Sullivan, M., Conley, A., Howell, D. A., et al. 2010, *MNRAS*, 406, 782, doi: [10.1111/j.1365-2966.2010.16731.x](https://doi.org/10.1111/j.1365-2966.2010.16731.x)
[x10.48550/arXiv.1003.5119](https://arxiv.org/abs/1003.5119)
- Taubenberger, S., Hachinger, S., Pignata, G., et al. 2008, *MNRAS*, 385, 75, doi: [10.1111/j.1365-2966.2008.12843.x](https://doi.org/10.1111/j.1365-2966.2008.12843.x)
- Taylor, G., Lidman, C., Tucker, B. E., et al. 2021, *MNRAS*, 504, 4111, doi: [10.1093/mnras/stab962](https://doi.org/10.1093/mnras/stab962)
- Thorp, S., & Mandel, K. S. 2022, *MNRAS*, 517, 2360, doi: [10.1093/mnras/stac2714](https://doi.org/10.1093/mnras/stac2714)
- Thorp, S., Mandel, K. S., Jones, D. O., Ward, S. M., & Narayan, G. 2021, *MNRAS*, 508, 4310, doi: [10.1093/mnras/stab284910.48550/arXiv.2102.05678](https://doi.org/10.1093/mnras/stab284910.48550/arXiv.2102.05678)
- Tonry, J., & Schneider, D. P. 1988, *AJ*, 96, 807, doi: [10.1086/114847](https://doi.org/10.1086/114847)
- Tripp, R. 1998, *A&A*, 331, 815
- Tully, R. B., & Fisher, J. R. 1977, *A&A*, 54, 661
- Uddin, S. A., Burns, C. R., Phillips, M. M., et al. 2020, *ApJ*, 901, 143, doi: [10.3847/1538-4357/abafb7](https://doi.org/10.3847/1538-4357/abafb7)
- . 2024, *ApJ*, 970, 72, doi: [10.3847/1538-4357/ad3e63](https://doi.org/10.3847/1538-4357/ad3e63)
- Verde, L., Treu, T., & Riess, A. G. 2019, *Nature Astronomy*, 3, 891, doi: [10.1038/s41550-019-0902-010-48550/arXiv.1907.10625](https://doi.org/10.1038/s41550-019-0902-010-48550/arXiv.1907.10625)
- Vincenzi, M., Brout, D., Armstrong, P., et al. 2024, *ApJ*, 975, 86, doi: [10.3847/1538-4357/ad5e6c](https://doi.org/10.3847/1538-4357/ad5e6c)
- Virtanen, P., Gommers, R., Oliphant, T. E., et al. 2020, *Nature Medicine*, 17, 261, doi: [10.1038/s41592-019-0686-2](https://doi.org/10.1038/s41592-019-0686-2)
- Wang, X., Li, W., Filippenko, A. V., et al. 2008, *ApJ*, 675, 626, doi: [10.1086/526413](https://doi.org/10.1086/526413)
- Wojtak, R., & Hjorth, J. 2022, *MNRAS*, 515, 2790, doi: [10.1093/mnras/stac1878](https://doi.org/10.1093/mnras/stac1878)
- . 2024, *MNRAS*, 533, 2319, doi: [10.1093/mnras/stae1977](https://doi.org/10.1093/mnras/stae1977)
- . 2025a, *A&A*, 702, A176, doi: [10.1051/0004-6361/202556288](https://doi.org/10.1051/0004-6361/202556288)
- . 2025b, *A&A*, 702, A176, doi: [10.1051/0004-6361/202556288](https://doi.org/10.1051/0004-6361/202556288)
- Wojtak, R., Hjorth, J., & Hjortlund, J. O. 2023, *MNRAS*, 525, 5187, doi: [10.1093/mnras/stad2590](https://doi.org/10.1093/mnras/stad2590)
- Zahid, H. J., Yates, R. M., Kewley, L. J., & Kudritzki, R. P. 2013, *ApJ*, 763, 92, doi: [10.1088/0004-637X/763/2/92](https://doi.org/10.1088/0004-637X/763/2/92)
- Zhang, X., & Green, G. M. 2025, *Science*, 387, 1209, doi: [10.1126/science.ado9787](https://doi.org/10.1126/science.ado9787)

APPENDIX

A. THE PANTHEON+ SAMPLE, TESTING COLOR DEPENDENCE

Here we show the result for different selections of color bins using Pantheon+. First, we split the sample into two bins, $c < 0$ and $c > 0$. Second, we calculate a $\Delta c = (c_{\text{cal,max}} - c_{\text{cal,min}})/N_{\text{bin}}$ of the entire color range covered by the calibration sample for different numbers of bins, $N_{\text{bin}} = 2, 3, 4, 5,$ and 6 , with $\Delta c = 0.133, 0.088, 0.066, 0.053$ and 0.044 , respectively. The results for both experiments are shown in Figures 7 and 8.

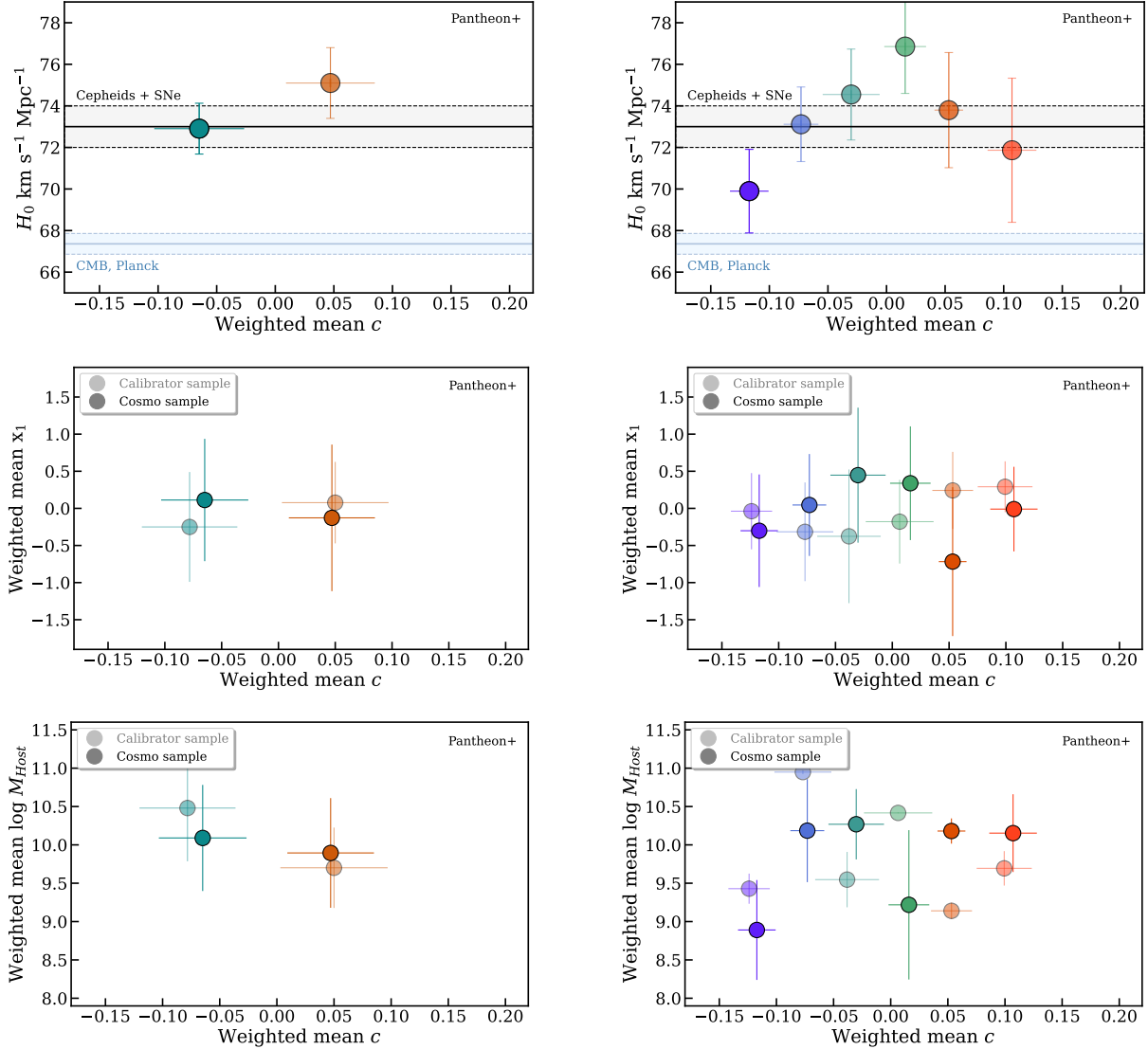


Figure 7. H_0 and mean lightcurve parameters for different color bins of the Pantheon+ data compilation. The left column shows the results of the dataset split into colors of $c < 0$ and $c > 0$. The right column shows the results of dataset split into six equal color bins. *Upper panels:* show H_0 . *Middle panels:* show the weighted mean SALT2 lightcurve shape parameter x_1 and standard deviation. *Lower panels:* show the weighted mean log host-galaxy mass and standard deviation.

Furthermore, to quantify the statistical significance of a potential dependence of H_0 on SN color, we perform a weighted linear regression of the form $H_0 = sc + p$, where s denotes the slope and p the intercept. The regression assumes independent 1σ uncertainties on H_0 , which are incorporated through a weighted least-squares likelihood.

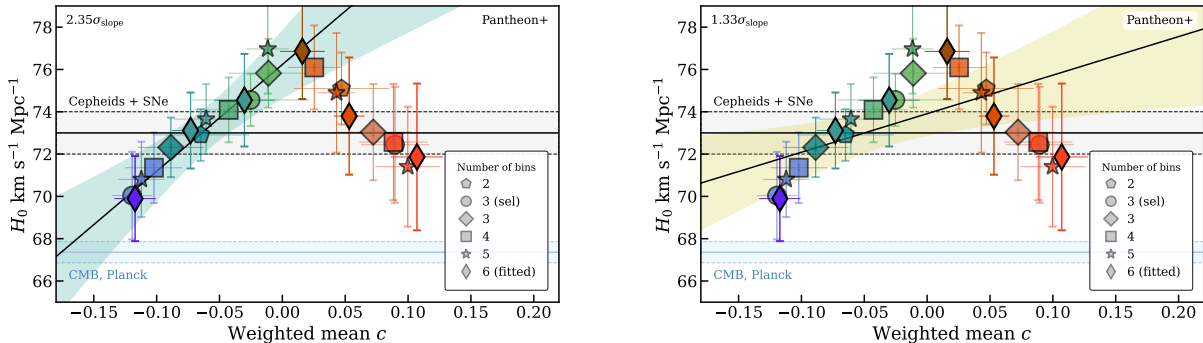


Figure 8. Testing H_0 color dependence from the Pantheon+ data compilation. Shown are H_0 values for different selections of equal color bins, such as 2, 3, 4, 5, and 6 indicated as pentagon, diamond, square, star, and thin diamond symbols, respectively. For comparison, the three color bins as selected in Sect. 3 are shown as circles. The blue and yellow shaded regions and black solid lines through them are the weighted linear regressions of the inferred Hubble constant H_0 as a function of mean supernova color c (6 bin case) using the pivot parameterization described in Section A. *Left:* fit to the four bluest color bins, yielding a slope significance of $2.35\sigma_s$. *Right:* fit to all six color bins, yielding a slope significance of $1.33\sigma_s$.

Since each H_0 measurement is derived from a distinct color bin constructed to avoid overlap of individual SNe, the measurements are treated as statistically independent to first order.

Model parameters are estimated using the Python routine `curve_fit` from the SciPy optimization library (Virtanen et al. 2020), which determines best-fit parameters through minimization of the chi-square statistic,

$$\chi^2 = \sum_i \frac{(H_{0,i} - H_{0,\text{model},i})^2}{\sigma_{H_{0,i}}^2}, \quad (\text{A1})$$

where $H_{0,\text{model},i} = sc_i + p$ and $\sigma_{H_{0,i}}$ is the 1σ uncertainty for each $H_{0,i}$. The algorithm employs a nonlinear least-squares solver based on the Levenberg–Marquardt method (Moré 1978). Under the assumption of locally Gaussian likelihood contours, the parameter covariance matrix returned by the fit is used to derive parameter uncertainties and correlations. To improve numerical stability and reduce covariance between the slope and intercept parameters, we adopt a pivoted form of the independent variable:

$$H_{0,i} = s(c_i - c_0) + p_c, \quad (\text{A2})$$

with c_0 as the mean color of the bins used in each regression, and p_c is the intercept evaluated at the pivot color. The standard intercept corresponding to $c = 0$ is recovered as $p = p_c - sc_0$.

This approach allows for a numerically stable estimation of both s and p , particularly when the dynamic range of c is small compared to the scale of H_0 . The slope s represents the sensitivity of the inferred H_0 to the mean supernova color, providing a direct probe of potential color-dependent systematic effects rather than a physical causal relation.

The stability of the inferred slope was validated using Monte Carlo realizations in which H_0 measurements were perturbed according to their uncertainties. The dispersion of recovered slopes is consistent with the parameter uncertainty derived from the covariance matrix returned by the χ^2 minimization, supporting the validity of the Gaussian error approximation adopted in the regression.

Figure 8 (left panel) shows the fit to the four bluest of six color bins, with a slope significance of $2.35\sigma_s$, suggestive of a possible color dependence of H_0 on the blue end. Including all six bins (Figure 8; right panel) results in a reduced slope significance of $1.33\sigma_s$. A fit restricted to the three reddest bins results in a slope significance of $1.26\sigma_s$, indicating that red SNe ($c > 0$) are consistent with a constant high H_0 within uncertainties. All regression parameters are summarized in Table 5.

B. CSP SAMPLE, TESTING COLOR DEPENDENCE

Similar to Pantheon+ in Sect. A, we show results for different color bins using the CSP sample. Similar to above, we calculate $\Delta(B - V) = ((B - V)_{\text{cal,max}} - (B - V)_{\text{cal,min}})/\text{bin}$, which results in $\Delta(B - V) \approx 0.16$ mag and $\Delta(B - V) \approx 0.08$ mag for bin=2 and bin=4, respectively. Furthermore, we test a simpler standardization in analogy to Khetan

et al. (2021) with

$$m_B = P^0 + P^1(s_{BV} - 1) + R(B_{\max} - V_{\max}) + \mu \quad (\text{B3})$$

and

$$\Gamma_X = \frac{(m_B - m_{B,model})^2}{\sigma_X^2}. \quad (\text{B4})$$

with σ_X^2 , as defined in Eq. 10 and 11 in Khetan et al. (2021), which includes an additional term for the intrinsic scatter, $\sigma_{\text{int},X}^2$. The total number of model parameters to be fit reduces to five (P^0 , P^1 , R , σ_{int} and H_0). We find that there is no significant difference in any of the fitted parameters of each color bin from either the complex model as employed in Uddin et al. (2024) or the simpler standardization similar to what is employed in Khetan et al. (2021). A comparison of the results of H_0 and R of the two models is shown in Figure 9, while the CSP model for four color bins is shown in Figure 10. Results of H_0 and R for an alternative binning with blue and red color cuts obtained using a mean peak color difference between the color distributions of the HF samples (Figure 1) of 0.04 (see Sect. 3), resulting in $c < -0.06$ (blue bin) and $c > 0.1$ (red bin) with green in between (Figure 11).

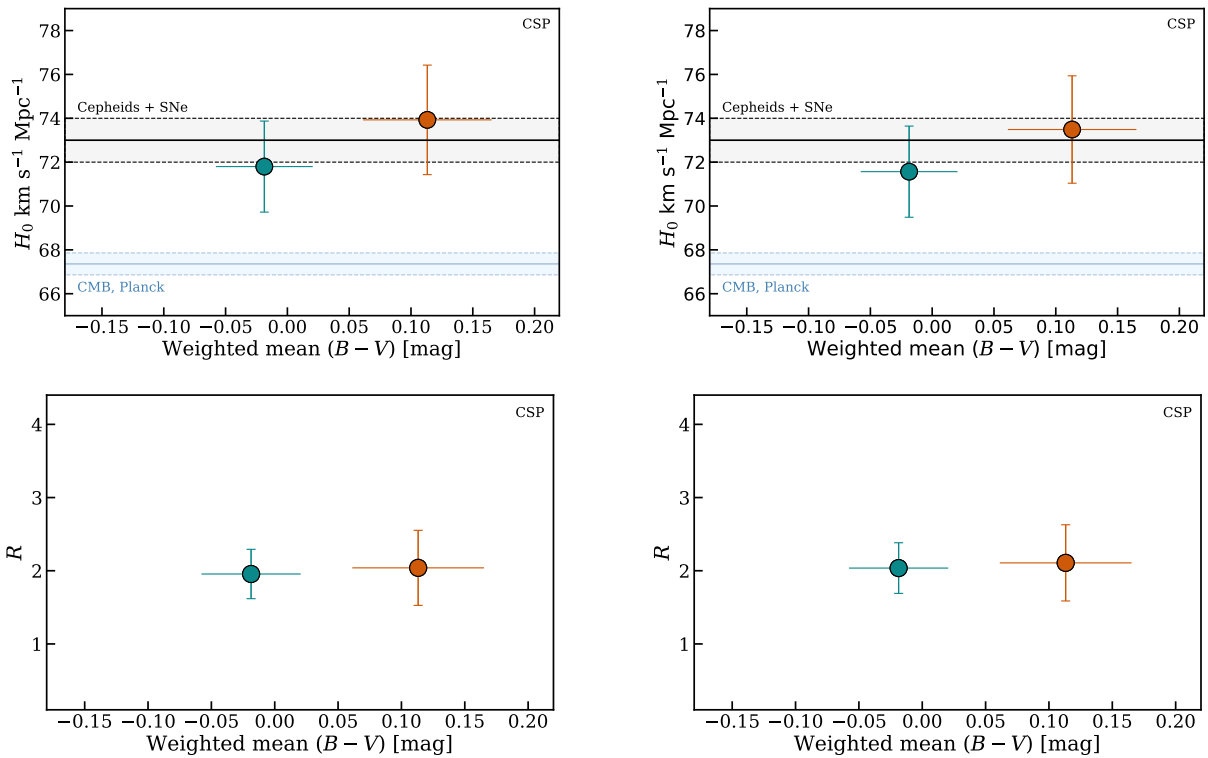


Figure 9. H_0 and R for two color bins and different models. The left column shows the results of the CSP data compilation split into color bins of $(B - V) < 0.0525$ and $(B - V) > 0.0525$. The right column shows the results of the same two color bins and for the simpler standardization as defined in Eq B3 and B4.

B.1. Testing Eddington Bias

As discussed in Sec. 3, here we test for Eddington bias using the same CSP setup with which results have been obtained, as shown in Figure 2. However, we only select SNe Ia which are including uncertainties within a color bin. This obviously leads to a reduction of the number of SNe Ia in each bin. The results, in comparison to what is also shown in Figure 2 are shown in Figure 12.

C. TABLES

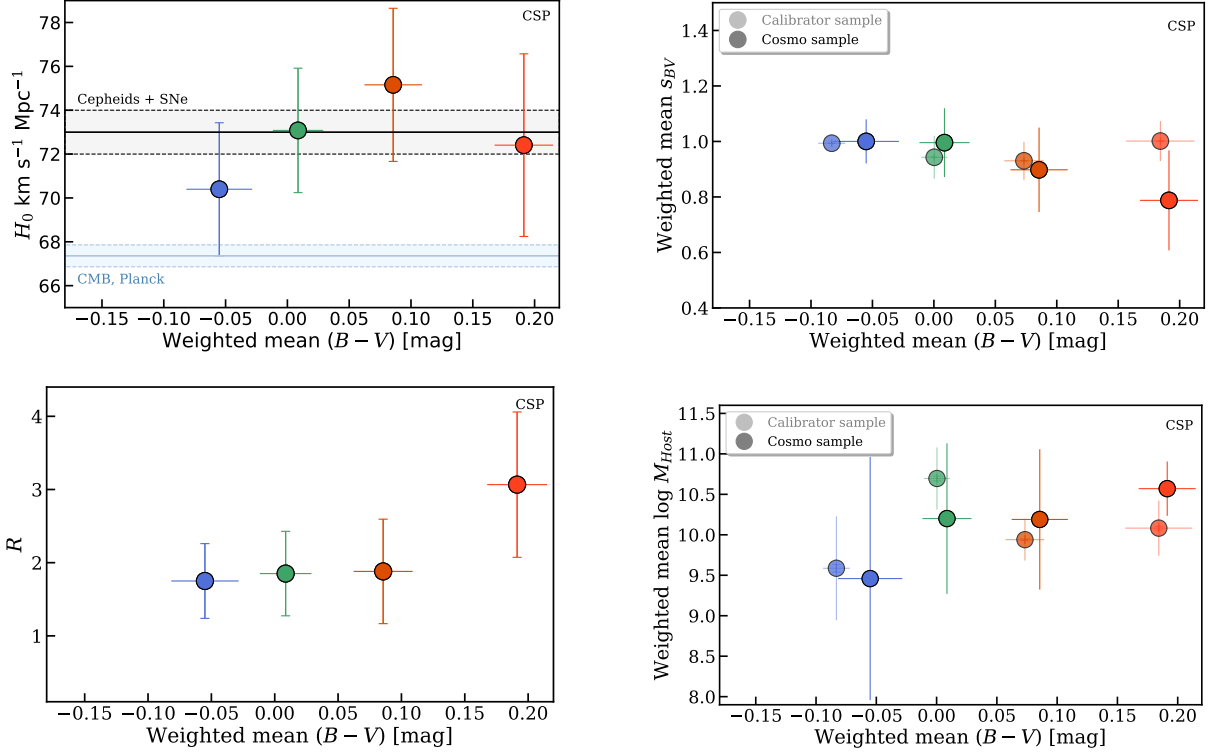


Figure 10. H_0 and mean lightcurve parameters for four color bins of CSP. Shown are the results for H_0 (upper left) and R (lower left), the weighted mean lightcurve shape parameter s_{BV} and standard deviation (upper right), and the weighted mean log host-galaxy mass and standard deviation (lower right).

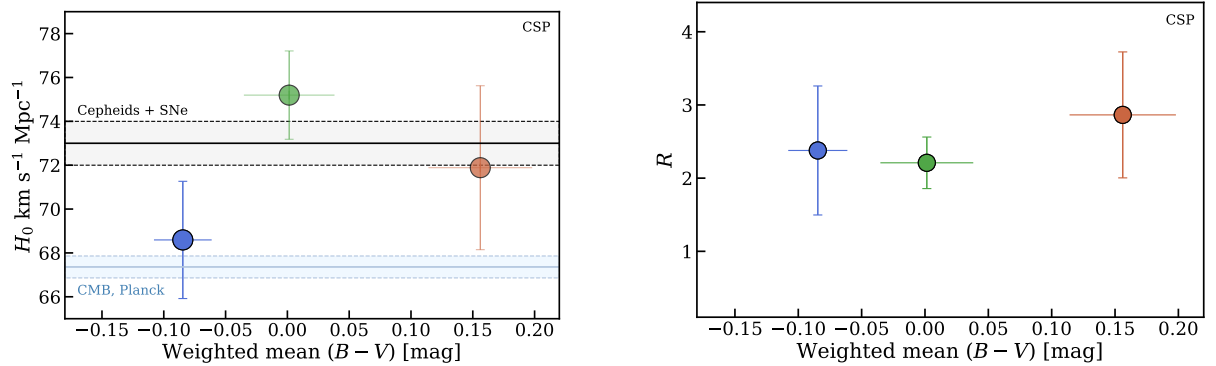


Figure 11. Alternative binning for CSP. *Left panel:* shown are the results of H_0 . *Right panel:* shown are the results of R . Color bin bounds are calculated using a mean peak color difference between the color distributions of the HF samples (Figure 1) of 0.04, resulting in $c < -0.06$ (blue bin) and $c > 0.1$ (red bin) with green in between.

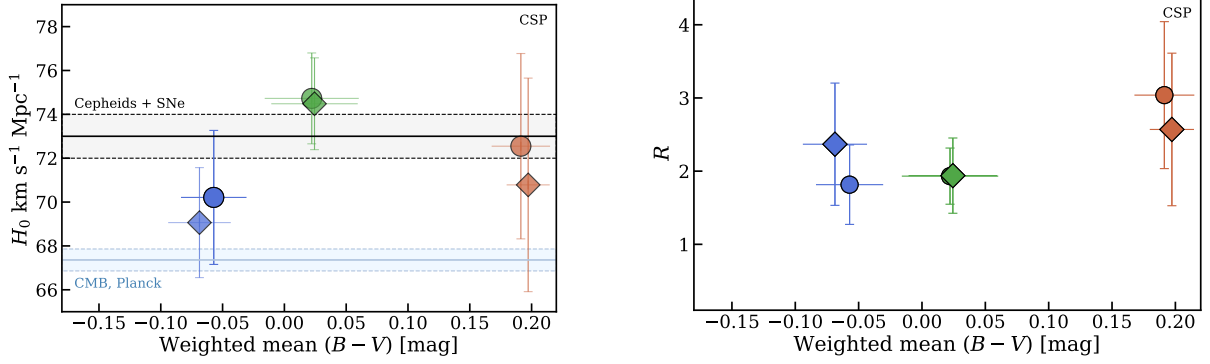


Figure 12. Testing Eddington bias for CSP. Shown are the results H_0 (left panel) and R (right panel). Squared symbols mark the model with SNe Ia within a color bin, including their uncertainties.

Table 3. Cosmological Tests with Different Data Sets: Pantheon+

Bin	M_b	H_0
Blue	-19.32(0.06)	69.98(2.08)
Green	-19.23(0.03)	74.51(1.23)
Red	-19.27(0.07)	72.47(2.72)

Table 4. Cosmological Tests with Different Data Sets: CSP

Bin	P^0	P^1	P^2	H_0	R	σ_{int}	vel_{pec}
Blue	-19.24(0.10)	-1.26(0.26)	2.0(1.77)	70.27(3.0)	1.8(0.55)	0.16(0.03)	525(319)
Green	-19.06(0.06)	-1.00(0.14)	0.65(0.80)	74.73(2.1)	1.9(0.40)	0.19(0.01)	180(133)
Red	-19.25(0.19)	-0.85(0.42)	0.39(2.02)	72.55(4.2)	3.04(1.00)	0.18(0.05)	713(493)

Table 5. Results of Pivot Linear Regression Tests for the Dependence of H_0 on SN Color.

Test	# Bins	Slope s	σ_s	c_{piv}	$H_{0,\text{piv}}$	$\sigma_{H_{0,\text{piv}}}$	p ($c=0$)	σ_p	Significance	Significance (MC)
Blue bins	4	50.46	21.46	-0.0569	73.36	1.02	76.23	1.59	2.35	2.34
Red bins	3	-56.58	44.93	0.0462	74.87	1.56	77.49	2.60	1.26	1.26
All bins	6	18.22	13.71	-0.0331	73.31	0.92	73.91	1.03	1.33	1.32

NOTE— c_{piv} denotes the pivot color corresponding to the weighted mean color of the SN sample used in each test. $H_{0,\text{piv}}$ represents the inferred Hubble constant evaluated at c_{piv} . The parameter p corresponds to the standard intercept evaluated at $c = 0$. Analytic uncertainties are derived from the covariance matrix of the weighted least-squares fit. Monte Carlo (MC) uncertainties are obtained from realizations of H_0 measurements perturbed according to their reported uncertainties. Significances are defined as s/σ_s .